Journal of Cerebral Blood Flow and Metabolism
20:225–243 © 2000 The International Society for Cerebral Blood Flow and Metabolism
Published by Lippincott Williams & Wilkins, Inc., Philadelphia

Measurement of Striatal and Extrastriatal Dopamine D_1 Receptor Binding Potential With [^{11}C]NNC 112 in Humans: Validation and Reproducibility

Anissa Abi-Dargham, Diana Martinez, Osama Mawlawi, Norman Simpson, Dah-Ren Hwang, Mark Slifstein, Satish Anjilvel, Justine Pidcock, Ning-Ning Guo, Ilise Lombardo, J. John Mann, Ronald Van Heertum, *Christian Foged, †Christer Halldin, and Marc Laruelle

*Departments of Psychiatry and Radiology, Columbia University College of Physicians and Surgeons, and Division of Brain Imaging, Department of Neuroscience, New York State Psychiatric Institute, New York, New York, U.S.A.; *Novo Nordisk, Malov, Denmark; and †Karolinska Institute, Stockholm, Sweden*

Summary: To evaluate the postulated role of extrastriatal D_1 receptors in human cognition and psychopathology requires an accurate and reliable method for quantification of these receptors in the living human brain. [^{11}C]NNC 112 is a promising novel radiotracer for positron emission tomography imaging of the D_1 receptor. The goal of this study was to develop and evaluate methods to derive D_1 receptor parameters in striatal and extrastriatal regions of the human brain with [^{11}C]NNC 112. Six healthy volunteers were studied twice. Two methods of analysis (kinetic and graphical) were applied to 12 regions (neocortical, limbic, and subcortical regions) to derive four outcome measures: total distribution volume, distribution volume ratio, binding potential (BP), and specific-to-nonspecific equilibrium partition coefficient (k_3/k_4). Both kinetic and graphic analyses provided BP and k_3/k_4 values in good agreement with the known distribution of D_1 receptors (striatum > limbic regions = neocortical regions > thalamus). The identifiability of outcome measures derived by kinetic analysis was excellent. Time–stability analysis indicated that 90 minutes of data collection generated stable outcome measures. Derivation of BP and k_3/k_4 by kinetic analysis was highly reliable, with intraclass correlation coefficients (ICCs) of 0.90 ± 0.06 (mean ± SD of 12 regions) and 0.84 ± 0.11, respectively. The reliability of these parameters derived by graphical analysis was lower, with ICCs of 0.72 ± 0.17 and 0.58 ± 0.21, respectively. Noise analysis revealed a noise-dependent bias in the graphical but not the kinetic analysis. In conclusion, kinetic analysis of [^{11}C]NNC 112 uptake provides an appropriate method with which to derive D_1 receptor parameters in regions with both high (striatal) and low (extrastriatal) D_1 receptor density. **Key Words:** Positron emission tomography—Dopamine—D_1 receptors—[^{11}C]NNC 112.

The D_1 receptors are the most abundant dopaminergic receptor subtype in neocortical areas including the prefrontal cortex (PFC) as well as in the hippocampus and amygdala (for reviews, see Seeman, 1992; Meador-Woodruff et al., 1996). Studies in nonhuman primates have shown that activation of D_1 receptors in the PFC is involved in working memory (Arnsten et al., 1994; Sawaguchi and Goldman-Rakic, 1994; Williams and Goldman-Rakic, 1995) and that D_1 receptors in the hippocampus are implicated in short- and long-term memory (Huang and Kandel, 1995; Otmakhova and Lisman, 1996; Bernabeu et al., 1997; Seamans et al., 1998). An accurate and reliable method for measuring these receptors in extrastriatal regions of the living human brain will permit the study of their role in mediating cognition in health and disease states.

The radiolabeled benzazepine [^{11}C]SCH 23390 (K_D = 0.4 nmol/L) was the first radiotracer developed to image the D_1 receptor with positron emission tomography (PET) (Billard et al., 1984; Halldin et al., 1986; Farde et al., 1987). Studies in humans have demonstrated

Received April 6, 1999; final revision received August 24, 1999; accepted August 24, 1999.

Supported by the National Alliance for Research in Schizophrenia and Depression, the Scottish-Rite Foundation, the Charles Dana Foundation, and the Public Health Service (NIMH K02 MH01603-0).

Address correspondence and reprint requests to Dr. Anissa Abi-Dargham, New York State Psychiatric Institute, 1051 Riverside Dr., Unit 42, New York, NY 10032, U.S.A.

Abbreviations used: AC-PC, anterior—posterior commissural; BP, binding potential; CSF, cerebrospinal fluid; CV, coefficient of variation; DLPFC, dorsolateral prefrontal cortex; DVR, distribution volume ratio; GM, gray matter; ICC, intraclass correlation coefficient; MRI, magnetic resonance imaging; OFC, orbitofrontal cortex; PET, positron emission tomography; PFC, prefrontal cortex; WM, white matter.

that [^{11}C]SCH 23390 is an appropriate radiotracer with which to measure D_1 receptors in the striatum, where these receptors are present in high density (Laihinen et al., 1994; Chan et al., 1998). However, [^{11}C]SCH 23390 displays relatively low specific/nonspecific ratios, which compromises the sensitivity and reliability of the D_1 receptor measurement in extrastriatal areas such as the PFC (Karlsson et al., 1997), where the density of these receptors is approximately fivefold lower than in the striatum (De Keyser et al., 1988; Laruelle et al., 1991; Hall et al., 1994).

Recently, two new benzazepines developed by Novo Nordisk (Malov, Denmark) (Andersen et al., 1992) have been evaluated as PET radiotracers in baboons: [^{11}C]NNC 756 (K_D = 0.17 nmol/L) and [^{11}C]NNC 112 (K_D = 0.18 nmol/L) (Halldin et al., 1993, 1998; Karlsson et al., 1993). Both radiotracers provide higher specific/nonspecific ratios than [^{11}C]SCH 23390. The disadvantage of [^{11}C]NNC 756 is a low selectivity against serotonin 5-HT_2 receptors. In baboons, ~25% of the binding of [^{11}C]NNC 756 in the frontal cortex was displaced by the 5HT_2 antagonist ketanserin (1.5 mg/kg) (Karlsson et al., 1993). In contrast, ketanserin injection (2 mg/kg) did not affect the frontal uptake of [^{11}C]NNC 112 (Halldin et al., 1998), indicating that [^{11}C]NNC 112 provides appropriate D_1/5-HT_2 selectivity *in vivo*. Thus, [^{11}C]NNC 112 appears as a promising candidate radiotracer with which to measure both striatal and extrastriatal D_1 receptors, and preliminary results in humans have confirmed the potential of this radiotracer (Halldin et al., 1998).

The purpose of the present study was to further evaluate [^{11}C]NNC 112 as a radiotracer with which to quantify D_1 receptors in the human brain. Specifically, the aim of this study was to define the optimal scanning protocol and analytic method to derive accurate and reliable D_1 receptor parameters in striatal and extrastriatal regions. Six healthy volunteers were studied twice, after injection of [^{11}C]NNC 112. Twelve brain regions were studied, ranging from high (caudate and putamen) to low (neocortex, limbic regions, and thalamus) receptor density regions. Two approaches were compared for measurement of D_1 receptor parameters: compartmental kinetic and graphical analysis. Four outcome measures were compared: total distribution volume (V_T), distribution volume ratio (DVR), binding potential (BP), and specific-to-nonspecific equilibrium partition coefficient (k_3/k_4). The comparison included four attributes of the outcome measures: their identifiability, which describes the degree of certainty in parameter estimation; validity, which is derived by comparison with *in vitro* values; stability, which evaluates the dependence of the outcome measures on the duration of the scan; and reliability, which is assessed with test/retest reproducibility studies.

MATERIALS AND METHODS

Human subjects

We report here the results of six consecutive weekly experiments. Six healthy volunteers participated in this study (age 33 ± 9 years, range 23 to 45 years; these and subsequent values given as means ± SD; five men and one woman). All subjects were scanned twice on the same day to evaluate the reproducibility of the outcome measures. The study was approved by the Columbia Presbyterian Medical Center Institutional Review Board, and subjects provided written informed consent after receiving an explanation of the study. The absence of pregnancy and medical, neurological, and psychiatric history (including alcohol and drug abuse) was assessed by history, review of systems, physical examination, routine blood tests including pregnancy test, urine toxicology, and electrocardiography.

Radiochemistry

[^{11}C]NNC 112 was prepared by *N*-methylation of the precursor using [^{11}C]methyltriflate as previously described (Halldin et al., 1998). Specific radioactivity at the time of injection was 1,255 ± 355 Ci/mmol (n = 12, range from 883 to 2,195 Ci/mmol). Injected dose was 15.0 ± 2.3 mCi (n = 12, range from 11.8 to 18.2 mCi).

Positron emission tomography protocol

Subject preparation included placement of arterial and venous catheters, fiducial markers, and polyurethane head immobilizer. An arterial catheter was inserted in the radial artery after completion of the Allen test and infiltration of the skin with 1% lidocaine. A venous catheter was inserted in a forearm vein on the opposite side. Four fiducial markers filled with ^{11}C (~3 μCi/marker at the time of injection) were glued on the subject's head. Head movement minimization was achieved with a polyurethane head immobilizer system (Soule Medical, FL, U.S.A.) molded around the head of the subject. This system provides better restraint than a thermoplastic mask (unpublished data). The PET imaging was performed with the ECAT EXACT 47 (Siemens/CTI, Knoxville, TN, U.S.A.; 47 slices covering an axial field of view of 16.2 cm, axial sampling of 3.375 mm, three-dimensional mode in-plane and axial resolution of 6.0 and 4.6 mm full width at half-maximum at the center of the field of view, respectively) (Wienhard et al., 1992). A 10-minute transmission scan was obtained before radiotracer injection. [^{11}C]NNC 112 was injected intravenously over 45 seconds. Emission data were collected in the three-dimensional mode for 120 minutes as 21 successive frames of increasing duration (3 × 20 s, 3 × 1 min, 3 × 2 min, 2 × 5 min, 10 × 10 min). Images were reconstructed to a 128 × 128 matrix (pixel size of 2.5 × 2.5 mm^2). Reconstruction was performed with attenuation correction using the transmission data and a Sheppe 0.5 filter (cutoff 0.5 cycle/projection rays). Subjects were allowed to rest outside of the camera for 15 to 30 minutes between the two injections.

Input function measurement

After radiotracer injection, arterial samples were collected every 5 seconds with an automated sampling system for the first 2 minutes (Graham and Lewellen, 1993) and manually thereafter at longer intervals. A total of 31 samples were obtained per experiment. After centrifugation (10 minutes at 1,800 *g*), plasma was collected in 200-μL aliquots and counted in a gamma counter (Wallac 1480 Wizard 3M Automatic Gamma Counter). Gamma counter efficiency was calibrated at regular intervals with the PET camera using an ^{18}F solution. In

addition, a long-lived source (^{22}Na) was counted with each set of samples to control for between-run variance in counting efficiency.

Six selected samples (collected at 2, 8, 16, 30, 50, and 70 minutes) were further processed by protein precipitation using acetonitrile followed by high-pressure liquid chromatography to measure the fraction of plasma activity representing unmetabolized parent compound. Plasma samples (0.5 mL) were added to 0.7 mL of acetonitrile in a centrifuge tube. After mixing, the samples were centrifuged at 14,000 rpm for 3.5 minutes. The acetonitrile solution was separated and analyzed by high-pressure liquid chromatography. The system consisted of a Waters 510 isocratic pump, a Rheodyne injector with a 2-mL loop, a Phenomenex C18 ODS column (10-μm particle size, 250 × 4.6 mm, stainless steel), and a gamma detection system (Bioscan Flow Count unit). The column was eluted with a solvent mixture of acetonitrile/0.1 mol/L aqueous ammonium formate (30:70) at a flow rate of 2.5 mL/min. Five fractions collected over 12 minutes were counted. A standard [^{11}C]NNC 112 solution was processed with each experiment. Parent eluted with fractions 3 and 4. For each sample, the fraction parent was estimated by the ratio of decay-corrected activity in collections 3 and 4 to that in the total collection.

A biexponential function was fitted to the six measured fractions parent and used to interpolate values between and after the measurements. The smallest exponential of the fraction parent curve, λ_{par}, was constrained to the difference between λ_{cer}, the terminal rate of washout of cerebellar activity, and λ_{tot}, the smallest elimination rate constant of the total plasma (Abi-Dargham et al., 1999). The input function was calculated by the product of total counts and interpolated fraction parent at each time. The measured input function values [$C_a(t)$; μCi/mL) were fitted to a sum of three exponentials, and the fitted values were used as input to the kinetic and graphical analyses. The clearance of the parent compound (C_L; L/h) was calculated as the ratio of the injected dose to the area under the curve of the input function (Abi-Dargham et al., 1994).

For the determination of the plasma free fraction (f_1), triplicate 200-μL aliquots of plasma collected before injection were mixed with radiotracer, pipetted into ultrafiltration units (Centrifree, Amicon, Danvers, MA, U.S.A.), and centrifuged at room temperature (20 minutes at 4,000 rpm). At the end of centrifugation, plasma and ultrafiltrate activities were counted, and f_1 was calculated as the ratio of ultrafiltrate to total activity concentrations (Gandelman et al., 1994). Triplicate aliquots of saline solution mixed with radiotracer were also processed to determine the filter retention of free [^{11}C]NNC 112.

Magnetic resonance imaging acquisition and segmentation procedures

Magnetic resonance imaging (MRI) was performed on a GE 1.5 T Signa Advantage system (Milwaukee, WI, U.S.A.). After a sagittal scout (localizer) image performed to identify the anterior–posterior commissural (AC-PC) plane (1 minute), a transaxial T1-weighted sequence with 1.5-mm slice thickness was acquired in a coronal plane orthogonal to the AC-PC plane over the whole brain with the following parameters: three-dimensional SPGR (spoiled gradient-recalled acquisition in the steady state); repetition time 34 milliseconds; echo time 5 milliseconds; flip angle 45°; slice thickness 1.5 mm and zero gap; 124 slices; field of view 22 × 16 cm; 256 × 192 matrix, reformatted to 256 × 256, yielding a voxel size of 1.5 × 0.9 × 0.9 mm; and time of acquisition 11 minutes.

The MRI segmentation was performed within MEDx (Sensor Systems, Sterling, VA, U.S.A.), with original subroutines implemented in MATLAB (Math Works, Natick, MA, U.S.A.). Steps for MRI segmentation included correction for field inhomogeneities, fitting of the voxel distribution to a combination of three Gaussians functions, voxel classification, and postfiltering. To correct for field inhomogeneity, histograms of one anterior coronal slice and one posterior coronal slice were computed, as described below. g_x was defined as the difference in peak locations divided by the distance between slices. In a similar manner, g_y was defined from two sagittal slices, and g_z was defined from two transaxial slices. Next, an image G was constructed of the same dimensions as the MR image, with G being an affine function with gradient (g_x, g_y, g_z). Gradient-corrected MRI of the image I was given by I/G. The principal advantage of this approach is that if there is no gradient inhomogeneity, the gradient correction causes no loss of resolution. Gradient-corrected images were then imported into MATLAB. Voxel intensity distribution was fit to a linear combination of three Gaussian functions:

$$N(x) = \sum_{k=1}^{3} \alpha_k \frac{1}{(\sqrt{2\pi\sigma_k})^{1/2}} \exp\left[-\frac{1}{2}\left(\frac{x-\mu_k}{\sigma_k}\right)^2\right] \quad (1)$$

where α_k, μ_k, and σ_k are the weight, mean, and SD of the Gaussian function for compartment k. The values of these parameters were estimated using maximum likelihood (Fig. 1), and the threshold values were used in the MEDx system to perform the segmentation of the MRI into gray matter (GM), white matter (WM), and cerebrospinal fluid (CSF) compartments. These thresholds were applied to create GM, WM, and CSF masks. The masks were finally smoothed and thresholded to remove isolated voxels.

Image analysis

Image analysis was performed with MEDx according to the following steps: frame realignment, PET-MRI registration, and time–activity curve measurement.

1. Frame realignment. To correct for head movement during the acquisition, all frames were coregistered to the first frame of the study, using a least-squares algorithm for

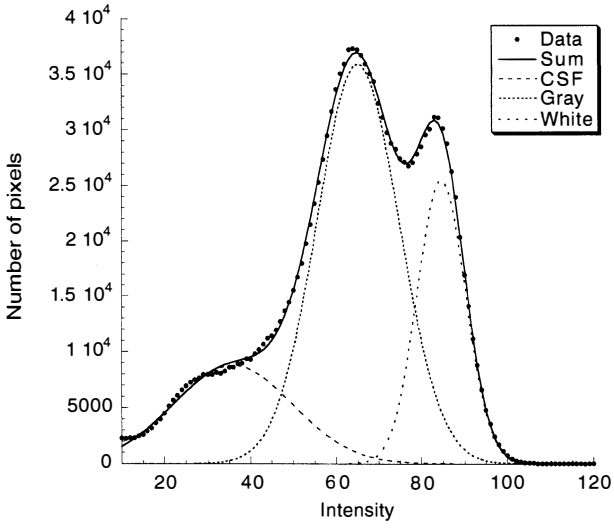

FIG. 1. Distribution of voxel intensity from a T1-weighted SPGR (spoiled gradient-recalled acquisition in the steady state) magnetic resonance imaging file and fitted sum of three Gaussians estimating voxel intensity of cerebrospinal fluid and gray and white matter. The solid line represents the sum of the fitted Gaussians. The intersection between the Gaussians was used as threshold for pixel classification.

within-modality coregistration (automated image registration) (Woods et al., 1992). Images were thresholded to the level of the ^{11}C fiducial markers, and only the signals from the markers were used for automated image frame-to-frame registration. The *x*, *y*, and *z* coordinates of the pixel with highest intensity of each fiducial marker were used to monitor the quality of between-frame coregistration.

2. PET-MRI registration. After frame-to-frame registration, the 21 frames were summed, and the summed PET image was coregistered and resampled to the MR image, using automated image registration (Woods et al., 1992). The summed PET image was used for the coregistration because it contains counts from the initial flow-dependent activity distributions that enhance detection of boundaries of regions with low receptor density, such as the cerebellum. The parameters of the spatial transformation matrix of the summed PET data set were then applied to each individual frame. Thus, each PET frame was resampled in the coronal plane to a voxel volume of $1.5 \times 0.9 \times 0.9$ mm^3.
3. Region-of-interest (ROI) tracing and activity sampling. The ROI boundaries were drawn on the MR image according to criteria based on brain atlases (Talairach and Tournoux, 1988; Duvernoy, 1991) and on published reports (Pani et al., 1990; Kates et al., 1997; Killiany et al., 1997). Neocortical regions included dorsolateral prefrontal cortex (DLPFC), medial prefrontal cortex, orbitofrontal cortex (OFC), anterior cingulate cortex, parietal cortex, temporal cortex, and occipital cortex. Subcortical regions included caudate, putamen, thalamus, amygdala, hippocampus, and cerebellum. Two methods were used for final ROI definition. A segmentation-based method was used for neocortical regions, and a direct identification method was used for subcortical regions. For neocortical regions, "large" regions were first drawn to delineate the boundaries of the ROIs. Within these regions, only the voxels classified as GM were used to measure activity distribution. This process is illustrated in Fig. 2 for DLPFC and OFC. Because of the mixture of GM and WM in central gray structures (especially thalamus), the segmentation-based approach was not used to define subcortical ROIs, and the boundaries of these regions were identified by anatomical criteria.

Quantitative analysis

Derivation of [^{11}C]NNC 112 regional distribution volumes was performed using kinetic and graphical analyses. A three-compartment model (i.e., two-tissue compartment model) provided the general framework for each method. The model included the arterial plasma compartment (C_a), the intracerebral free and nonspecifically bound compartment (nondisplaceable compartment; C_2), and the specifically bound compartment (C_3). The equilibrium distribution volume of a compartment *i* (V_i; mL/g) was defined as the ratio of the tracer concentration in this compartment to the free plasma concentration at equilibrium:

$$V_i = \frac{C_i}{f_1 C_a} \quad (2)$$

V_2 and V_3 were defined as the distribution volumes of the second (nondisplaceable) and third (specific) compartments, respectively. V_3 is equal to BP (g/mL), which is the ratio of the receptor density (B_{max}; nmol/L/g of tissue) and affinity (K_D; nmol/L/mL of brain water) (Mintun et al., 1984; Laruelle et al., 1994*d*). V_T was defined as the total regional equilibrium distribution volume, equal to the sum of V_2 and V_3. Both kinetic and graphical analyses shared two assumptions: given the negligible concentration of D_1 receptors in the cerebellum (Hall et al., 1994), cerebellar V_T was assumed to represent only free and nonspecific binding and to provide a reasonable estimate of V_2 in the ROIs; the contribution of plasma total activity to the regional activity was calculated assuming a 5% blood volume in the ROIs (Mintun et al., 1984).

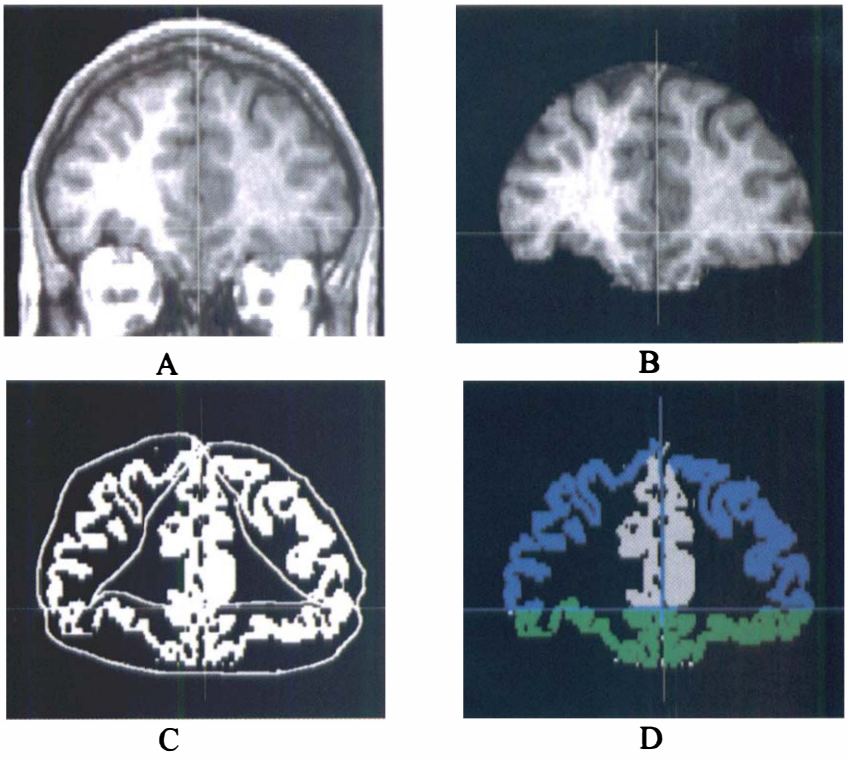

FIG. 2. The process of region-of-interest (ROI) definition for dorsolateral prefrontal cortex (DLPFC) and orbitofrontal cortex (OFC) in one coronal plane. **(A)** Original magnetic resonance (MR) image [coronal plane, perpendicular to anterior–posterior commissural (AC-PC) plane, 5 mm anterior to the anterior part of the genu of corpus callosum]. The vertical line is the midsagittal section, and the horizontal line is the AC-PC plane. **(B)** MR image after removal of extracerebral tissue. **(C)** Same image as B after segmentation, with only gray matter (GM) represented. Lines represent boundaries of ROIs. Two ROIs are defined on each side: Above the AC-PC plane and excluding the medial gray is the DLPFC. Below the AC-PC plane is the OFC. **(D)** GM voxels are assigned to ROIs if included within ROI boundaries: blue, DLPFC; green, OFC.

Kinetic analysis

Kinetic analysis was performed according to the differential equations:

$$\frac{dC_2(t)}{dt} = K_1 C_a(t) - k_2 C_2(t) - k_3 C_2(t) + k_4 C_3(t) \quad (3)$$

$$\frac{dC_3(t)}{dt} = k_3 C_2(t) - k_4 C D_3(t) \quad (4)$$

with the kinetic parameters defined as

$$K_1 = FE = F(1 - e^{-PS/F}) \qquad (\text{mL g}^{-1}\ \text{min}^{-1}) \quad (5)$$

$$k_2 = \frac{K_1}{V_2 f_1} \qquad (\text{min}^{-1}) \quad (6)$$

$$k_3 = \frac{k_{on} B_{max}'}{V_2} \qquad (\text{min}^{-1}) \quad (7)$$

$$k_4 = k_{off} \qquad (\text{min}^{-1}) \quad (8)$$

where F (mL g^{-1} min^{-1}) is the regional blood flow, E (unitless) the unidirectional extraction fraction, PS (mL g^{-1} min^{-1}) the permeability–surface area product of the tracer, k_{on} [(nmol/L)$^{-1}$ min^{-1}] the bimolecular ligand–receptor association rate constant, B_{max}' (nmol/L) the concentration of receptors available for binding (equal to B_{max} as experiments were performed at tracer dose), and k_{off} (min^{-1}) the receptor dissociation rate constant. Kinetic parameters were derived by nonlinear regression using a Levenberg–Marquart least-squares minimization procedure (Levenberg, 1944) implemented in MATLAB, as previously described (Laruelle et al., 1994*c*). In the absence of precise knowledge of the variance associated with the measurement of each frame, uniform weighting was used in the regression (Carson, 1986; Burger and Buck, 1997). Goodness of fit of models with different levels of complexity was compared using the Akaike information criterion (Akaike, 1974) and the F test (Landlaw and DiStefano, 1984; Carson, 1986).

In the ROIs, volumes of distribution were then calculated according to

$$V_2 = \frac{K_1}{k_2 f_1} \quad (9)$$

and

$$V_3 = \frac{K_1 k_3}{k_2 k_4 f_1} = \text{BP} \quad (10)$$

Substituting in Eq. 10 the terms $K_1/k_2 f_1$, k_3, and k_4 with Eqs. 5, 6, and 7, respectively, and recalling that $K_D = k_{off}/k_{on}$ establish the equivalence between V_3 and BP (Laruelle et al., 1994*a*).

The BP, as defined above, is the only expression of BP that is dependent on receptor parameters (i.e., K_D and B_{max}) and can be compared with *in vitro* values (see derivations in Laruelle et al., 1994*a*). Another outcome measure of interest is the specific-to-nonspecific equilibrium partition coefficient, termed k_3/k_4 or V_3'' (Laruelle et al., 1994*d*):

$$\frac{k_3}{k_4} = \frac{\text{BP}}{V_2} \quad (11)$$

k_3/k_4 is often used as the outcome measure in the PET literature and is referred to as the BP (Gjedde and Wong, 1990; Logan et al., 1990). In fact, this ratio does not correspond to BP ($= B_{max}/K_D$) as classically defined by Mintun et al. (1984) but to the ratio of BP to V_2, as shown by dividing Eq. 10 by Eq. 9 (Eq. 11). To avoid confusion, we use BP to designate the "true" BP, as defined in Eq. 10, and k_3/k_4 to designate the "practical" BP, as defined in Eq. 11.

The ratio of total to nonspecific distribution volume is termed the DVR:

$$\text{DVR} = \frac{V_T}{V_2} = \frac{k_3}{k_4} + 1 \quad (12)$$

DVR is reported to facilitate comparison with results of studies reporting reproducibility of [^{11}C]raclopride DVR (Volkow et al., 1993), [^{18}F]altanserin DVR (Smith et al., 1998), and [^{11}C]SCH 23390 DVR (Chan et al., 1998).

Results from kinetic analysis were evaluated with four criteria: identifiability, validity, stability, and reliability.

1. Identifiability. The term "identifiability" refers to the error in the parameter estimation due to the inherent uncertainty of this estimation. The identifiability was assessed by the standard error of the parameter at convergence. The standard error of the parameters was given by the diagonal of the covariance matrix (Carson, 1986) and expressed as percentage of the parameters (coefficient of variation; %CV). This standard error should not be confused with the variance of the parameter in the investigated population (between-subject SD or %CV) or with the lack of reproducibility (within-subject SD or %CV). It should also be noted that uniform weighting of the least-squares estimation might be associated with an overestimation of the standard error of the parameters if the measurement variances range over orders of magnitude (Carson, 1986).
2. Validity. Physiological plausibility was assessed by comparing regional BP values with distribution of D_1 receptors in the human brain *in vitro,* as reported by De Keyser et al. (1988), who used autoradiography and [^{3}H]SCH 23390 in the presence of 20 nmol/L mianserin to preclude binding to 5-$HT_{2A/2C}$ receptors, and Hall et al. (1988), who used homogenized membranes, [^{3}H]SCH 23390, and 40 nmol/L ketanserin.
3. Stability. Experimental data were collected for 120 minutes. The relationship between BP derivation and the duration of the scan was evaluated by fitting shorter-duration data sets (110, 100, 90, 80, 70, 60, 50, 40, and 30 minutes) and comparing the results with the reference value obtained with the 120-minute data set. For each region and each duration, the averages ± SD (n = 12) of the results expressed as percentage of the reference value were calculated to provide an estimate of the bias (average) or dispersion (SD) induced in the outcome measure by analyzing shorter data sets. The solution was considered stable after time t if all results derived from time t to the end of the experiment had a mean within 10% of the reference value and an SD that did not exceed 15%.
4. Reliability. The test/retest variability was calculated as the absolute value of the difference between test and retest values, expressed as percentage of the mean value of both measurements. To evaluate the within-subject variability relative to the between-subject variability, both within-subject SD and between-subject SD were calculated and expressed as percentage of mean value (within-subject %CV and between-subject %CV). The reliability of the measurements was assessed by the intraclass correlation coefficient (ICC) calculated as follows (Kirk, 1982):

$$\frac{\text{BSMSS} - \text{WSMSS}}{\text{BSMSS} + (\text{n} - 1)\,\text{WSMSS}} \quad (13)$$

where BSMSS is the mean sum of squares between subjects, WSMSS is the mean sum of squares within subjects, and n is the number of repeated observations (n = 2 in this study). This coefficient estimates the reliability of the measurement and assumes values from −1 (no reliability; i.e., BSMSS = 0) to 1 (maximum reliability, achieved in case of identity between test and retest; i.e., WSMSS = 0).

Graphical analysis

Regional time–activity curves were graphically analyzed according to the equation

$$\frac{\int_0^t C_{\text{ROI}}(t)dt}{C_{\text{ROI}}(t)} = a\frac{\int_0^t f_1 C_a(t)dt}{C_{\text{ROI}}(t)} + b \quad (14)$$

where the values of the slope a and the intercept b were obtained by linear regression (Logan et al., 1990). This method allows the determination of regional V_T of reversible ligands as the slope of the regression line without assuming a particular compartmental configuration. Assuming, as in the kinetic analysis, the equivalence between the cerebellum distribution volume ($V_{T\,cer}$) and the nondisplaceable distribution volume in the ROI, outcome measures were calculated as

$$\text{BP} = V_{T\,\text{ROI}} - V_{T\,\text{cer}} \quad (15)$$

$$\text{DVR} = \frac{V_{T\,\text{ROI}}}{V_{T\,\text{cer}}} \quad (16)$$

and

$$\frac{k_3}{k_4} = \text{DVR} - 1 \quad (17)$$

Reliability of the graphical analysis was evaluated as described for the kinetic analysis.

Noise analysis

Simulations were performed to evaluate the sensitivity of the kinetic and graphical analysis to experimental noise. This analysis was carried out for the cerebellum and one ROI (caudate). First, noise-free data [$T(t)$] were created, using a standard input function and a standard impulse response function. Data were simulated for 120 minutes, with values calculated every minute (n = 120). Second, various levels of random noise were introduced into the data. Due to the rapid decay of ^{11}C, the noise increased over the course of an experiment, and the simulated noise was designed to reflect this effect. For noise level $\{\alpha_j\}$, a normal random noise vector with mean 1 and SD at time t equal to α_j[exp(τt)/SD of exp(τt)] was generated, where τ was the exponent associated with ^{11}C half-life [20 minutes, τ = 0.034 = ln (2)/20]. The "true" datum $T(t)$ was multiplied at each point by the noise vector, resulting in a "measured" data set $M(t)$ with mean = $T(t)$ and SD$j(t)$ = $T(t)\alpha_j$[exp(0.034t)/SD of exp(τt)]. At each noise level α_j, this operation was repeated 500 times. Each data set was analyzed with kinetic or graphical analysis. The average V_T derived from these noisy data sets was compared with the true value to estimate the bias introduced by the noise in the derivation of V_T, whereas the SD provided a measure of the noise-related error in V_T.

Statistical analysis

For each outcome measure and each subject (n = 6), the average of test and retest values was calculated, and results are given as means ± SD of these six average measurements. Thus, unless otherwise specified, SD refers to between-subject SD, that is, to the estimated variability in the investigated population (each subject counts only once, n = 6). When the SD refers to variability between the experiments rather than between subjects (such as for the injected dose), the SD is followed by n = 12. Statistical analysis was performed with repeated-measures analysis of variance. Relationships between continuous variables were analyzed with the Pearson product–moment correlation coefficient. A two-tailed probability value of 0.05 was selected as the significance level.

RESULTS

Plasma analysis

[^{11}C]NNC 112 underwent rapid metabolism measured in human plasma (Fig. 3). At 30 minutes, only 18 ± 6% (n = 12) of the total activity corresponded to the parent compound. The six measures (2, 8, 16, 30, 50, and 70 minutes) of fraction parent were fit to a sum of two exponentials. In all cases, the unconstrained fit of the fraction parent curve yielded a value of 0 for the smallest exponent (λ_{par}). This solution was consistent with the low rate of metabolism after 30 minutes and the absence of data after 70 minutes. However, this solution was not consistent with the observation of a faster washout rate in the cerebellum compared with the total plasma activity after 30 minutes. This problem was addressed by constraining λ_{par} to the difference between λ_{cer}, the terminal rate of washout of cerebellar activity, and λ_{tot}, the smallest elimination rate constant of the total plasma. For each experiment, the terminal cerebellar washout rates were calculated by fitting the cerebellum data from 30 to 120

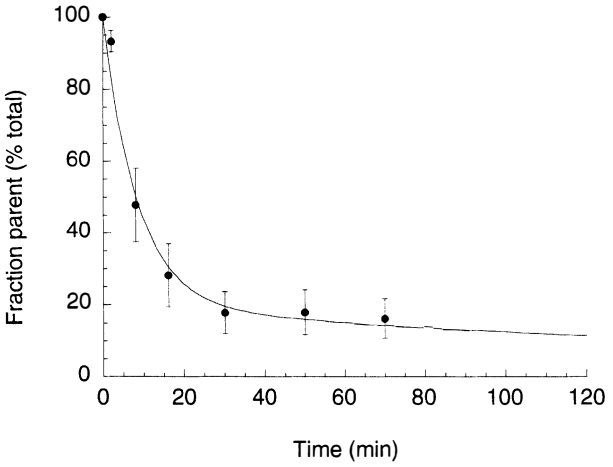

FIG. 3. Fraction of plasma activity associated with parent compound (% total) following [^{11}C]NNC 112 injection in humans. Each point is the average ± SD of 12 measurements (6 subjects studied twice). The solid line represents the sum of two exponentials, with second half-life constrained to −0.00440 min^{-1}. This value corresponded to the average value of the difference between cerebellum and total plasma terminal half-lives.

minutes to a one-exponential function (λ_{cer} = −0.00764 ± 0.00287 min^{-1}, n = 12). Similarly, the smallest exponential of the total plasma activity was derived by fitting the total plasma activity from 30 to 120 minutes to one exponential (λ_{tot} = −0.00322 ± 0.00083 min^{-1}, n = 12). The smallest exponential of the fraction parent curve was constrained to the difference between the two functions λ_{cer} and λ_{tot} (−0.00450 ± 0.00296 min^{-1}, n = 12), and this fit was used to correct total activity by the fraction parent.

The input function was fit to a sum of three exponentials (Fig. 4), and fitted values were used as input function for kinetic and graphical analysis. The average [^{11}C]NNC 112 plasma clearance was 96 ± 31 L/h. Significant between-subject differences in plasma clearance were detected (P = 0.006). Test/retest variability of the clearance measurement was 15 ± 8%, and its reliability was excellent with within-subject %CV of 10%, between-subject %CV of 32%, and ICC of 0.83.

The mean plasma f_1 fraction was 1.02 ± 0.28%. The within-subject CV of the f_1 measurement (34% CV) exceeded the between-subject CV (27%), which translated into poor reliability (ICC = −0.20). In addition, significant retention of free radiotracer on the filter was noted (the free fraction measured in saline solution was 77 ± 4%, n = 12). Because of the failure to reliably identify between-subject differences in free fraction, this correction factor was neglected, and distribution volumes were expressed relative to the total parent.

Brain uptake

Highest brain regional uptake was observed in caudate and putamen, and lowest uptake was observed in the cerebellum and thalamus (Fig. 5). In other regions (neocortex and limbic system), activity levels were intermediate between striatal and cerebellar regions. Activity peaked early in the cerebellum, neocortical, and limbic regions (<15 minutes) and later in striatum (20–40 minutes). Appreciable washout was observed in all regions, suggesting that the association and dissociation rates were fast enough to allow derivation of D_1 receptor BP within the time frame of the scan. At 60 minutes, the ROI/cerebellar activity ratios were as follows: putamen, 3.72 ± 0.58; caudate, 3.26 ± 0.58; amygdala, 1.77 ± 0.32; hippocampus, 1.48 ± 0.23; anterior cingulate, 1.78 ± 0.29; DLPFC, 1.53 ± 0.20; temporal cortex, 1.69 ± 0.33; occipital cortex, 1.30 ± 0.17; and thalamus, 1.19 ± 0.21.

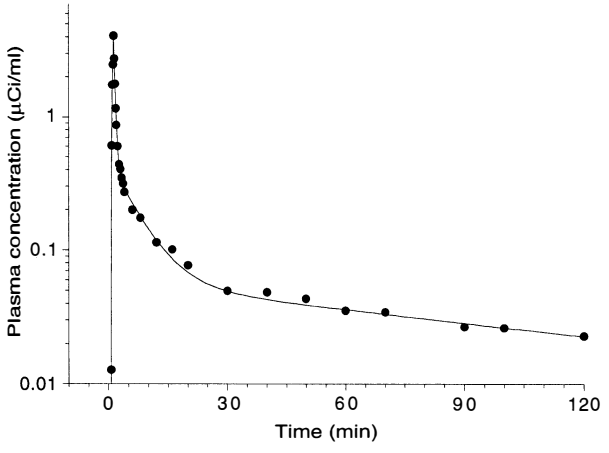

FIG. 4. Plasma concentration of [^{11}C]NNC 112 following injection of 18 mCi in one healthy volunteer. Points represent measured values. The solid line represents the result of a three-exponential fit to the measured values. Clearance was 100 L/h.

Kinetic analysis

Cerebellum. Cerebellar time–activity curves were fit to both a two- and a three-compartment model. In all cases, the three-compartment model provided a slightly but significantly better fit (P < 0.01; Fig. 6), with smaller values of Akaike information criterion (data not shown). Cerebellum V_T values calculated with the two- and three-compartment models were 2.54 ± 0.42 and 3.41 ± 0.58 mL g^{-1}, respectively. Thus, cerebellar V_T was 43% larger when calculated with a three-compartment model than a two-compartment model. The improved goodness of fit of the three-compartment model favored this model. However, several other factors favored the two-compartment model: (1) The identifiability of cerebellar V_T derived with a two-compartment model analysis (error of 4.13 ± 1.0%) was superior to that of the three-compartment model analysis (9.52 ± 7.13%). (2) The cerebellar V_T values derived by the Logan analysis (2.75 ± 0.48 mL g^{-1}) were closer to the two-compartment model cerebellar V_T (2.54 ± 0.42 mL g^{-1}) than the three-compartment model cerebellar V_T (3.41 ± 0.58 mL g^{-1}). (3) The stability over time of the two-compartment model was superior to that of the three-compartment model: For the two-compartment model, all values derived for periods from 60 to 120 minutes were within 10% of the reference value (=120-minute value). In contrast, values were very unstable for the three-compartment model, with no discernible pattern over time and large standard errors (Fig. 7). (4) Derivation of cerebellar V_T by the two-compartment model was very reproducible. The test/retest variability and reliability of the two-compartment model V_T (test/retest variability = 6 ± 6%, between-subject %CV = 17%, within-subject %CV = 3%, ICC = 0.92) were much better than for the three-compartment model V_T (test/retest variability = 21 ± 23%, between-subject %CV = 17%, within-subject %CV = 19%, ICC = −0.10). Together, these data suggest that the three-compartment model cerebellar fit was unstable and sensitive to the noise associated with cerebellar measurements at the end of the experiments. For these reasons, the two-compartment model fit was selected as the fit of choice to derive cerebellar V_T.

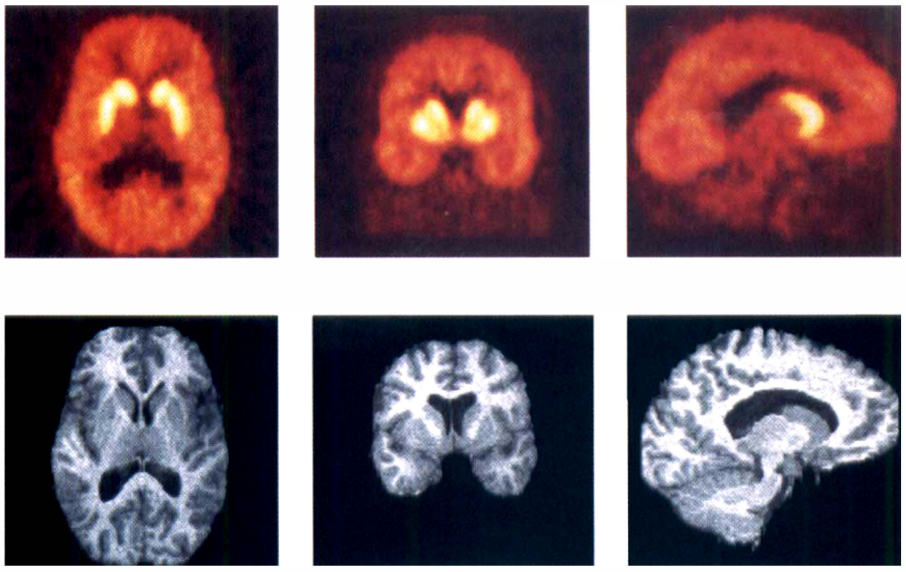

FIG. 5. [^{11}C]NNC 112 in a human volunteer. (**Top row**) Positron emission tomography: Transaxial, coronal, and sagittal views of a 20-minute frame obtained 40 minutes after the injection of 16 mCi of [^{11}C]NNC 112 in a 22-year-old man. (**Bottom row**) Magnetic resonance imaging: SPGR (spoiled gradient-recalled acquisition in the steady state) acquisitions in the corresponding planes. Activity is concentrated in caudate, putamen, neocortex, and hippocampus. Background activity is measured in the cerebellum. Thalamic activity is very low. This distribution corresponds to the anatomical distribution of the dopamine D_1 receptors.

Regions of interest. Data from all the other regions were fitted to a three-compartment model, with the K_1/k_2 ratio constrained to the value of the cerebellum V_T (two-compartment model). Results are presented in Table 1. The BP ranged from 8.44 ± 2.57 mL g^{-1} (putamen) to 1.45 ± 0.41 mg g^{-1} (thalamus). Despite these large regional differences in D_1 receptor density, the constrained model performed well in all regions.

Identifiability. Overall, the goodness of fit was excellent, and V_T values were well identified. Regional V_T mean identifiability was 5.75 ± 6.25% (n = 144, range from 2.60 ± 0.69% in the putamen to 10.6 ± 8.43% in the hippocampus). The BP values were also well identified, with slightly more uncertainty in small-size regions (hippocampus and amygdala) or regions with lower D_1 receptor density (thalamus). The BP mean identifiability was 11.9 ± 13.0% (n = 144, range from 3.42 ± 0.98% in putamen to 24.4 ± 16.7% in thalamus). The K_1 values were very well identified in all regions (2.36 ± 0.45%, n = 144, range from 1.60 ± 0.65% in temporal cortex to 3.03 ± 1.24% in caudate). A larger but still acceptable uncertainty was associated with values of k_3 (23.4 ± 16.3%, n = 144) and k_4 (33.5 ± 27.6%, n = 144). The k_3/k_4 ratios were well identified (12.9 ± 16.1%, n = 144).

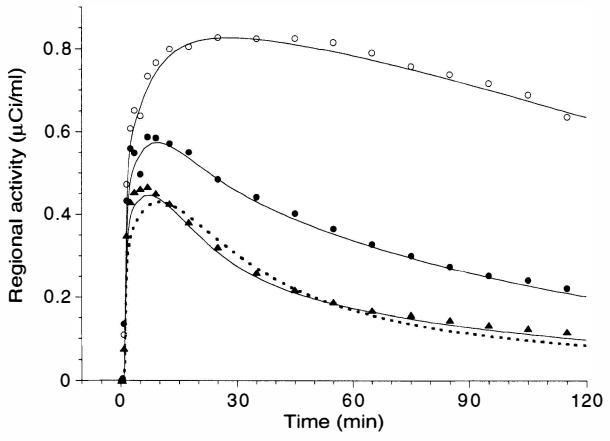

FIG. 6. Brain time–activity curves measured in putamen (open circles), dorsolateral prefrontal cortex (filled circles), and cerebellum (triangles) after injection of 18 mCi of [^{11}C]NNC 112 (same subject as in Fig. 4). The solid line represents the results of a three-compartment model fit, and the dashed line illustrates a two-compartment model fit in the cerebellum. In the cerebellum, the three-compartment model provided a slightly but significantly better fit.

Validity. A significant relationship was observed between PET and autoradiography measures (r^2 = 0.97, P < 0.001) and between PET and homogenate membrane measures (r^2 = 0.94, P < 0.001) (Table 2).

Stability. The ROI time–activity curves were fit to shorter scanning time durations, and BP values derived from shorter scanning times were expressed relative to BP values derived with 120-minute scanning time. Average BP values were 101 ± 8% at 105 minutes (n = 120, 12 regions × 10 scans), 102 ± 8% at 95 minutes, 104 ± 8% at 85 minutes, 117 ± 42% at 75 minutes, and >120% for shorter scanning times. At 85 minutes (corresponding to a total scanning time of 90 minutes), all regions were within 10% of the reference value, with the exception of the thalamus (112 ± 30%). Figure 8 displays time–stability analyses of the caudate and the DLPFC.

Reproducibility. The reproducibility of regional V_T and DVR are presented in Table 3. For each outcome measure, Table 3 lists the regional mean, between-subject SD (%CV), within-subject SD (%CV), test/retest variability, and ICC. For each outcome measure and each region, the between-subject SD exceeded the within-subject SD (Fig. 9). The test/retest variabilities of V_T and DVR were 8 ± 2 and 6 ± 2%, respectively. The ICC of V_T (0.91 ± 0.06) was slightly but significantly better than

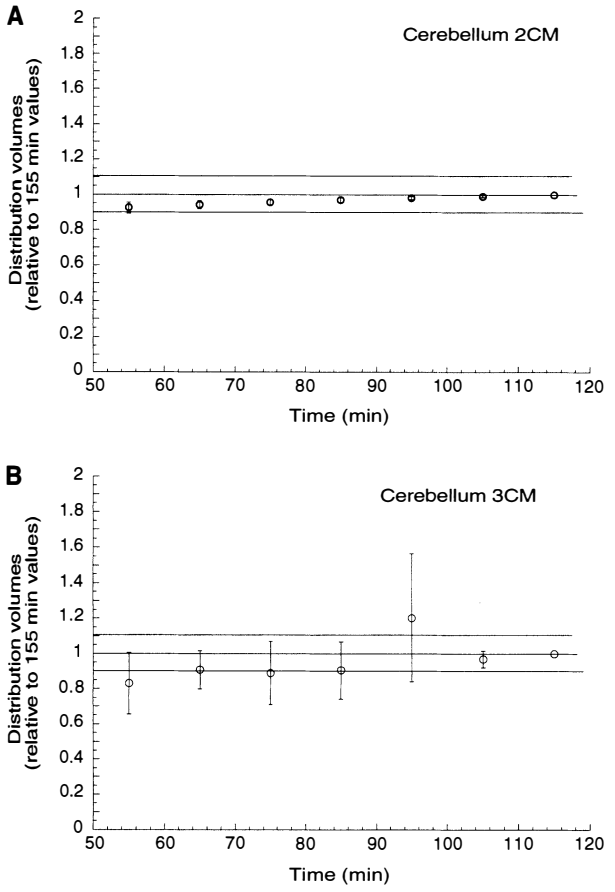

FIG. 7. Relationship between duration of data collection and kinetic derivation of total distribution volume (V_T) in the cerebellum, according to two-compartment model **(A)** and three-compartment model **(B)**. V_T values were normalized to the reference value, defined as the value measured with the whole data set (120 minutes of data collection). Each time point represents the mean ± SD of 12 determinations (6 subjects studied twice). With the two-compartment model, all values after 50 minutes were located within ±10% of the reference values (filled columns), and the SD was very low. This result indicated that the cerebellum V_T derivation with the two-compartment model was stable and, for times of >50 minutes, practically independent of the scanning duration. In contrast, the three-compartment model presented larger deviations from the reference values, and the SD was much larger than with the two-compartment model, indicating lack of stability of the results.

the ICC of DVR (0.84 ± 0.10, paired t test, $P = 0.0409$). The reproducibility of BP and k_3/k_4 is presented in Table 4. The test/retest variability of BP (14 ± 5%) and k_3/k_4 (13 ± 5%) was comparable and larger than for V_T (8 ± 2%) and DVR (6 ± 2%). However, for both measures, the between-subject SD exceeded the within-subject SD and the reliability was excellent (BP ICC = 0.90 ± 0.06, k_3/k_4 ICC = 0.84 ± 0.11). The reliability of BP compared with k_3/k_4 was significantly better (paired t test, $P = 0.017$).

Graphical analysis

By visual inspection, Logan plots achieved linearity at times of >25 minutes, and a linear regression was performed on data from the 30- to 120-minute interval (Fig. 10). The V_T, BP, DVR, and k_3/k_4 values derived from graphical analysis are listed in Table 5. Regional V_T derivedby the graphical method was highly correlated with V_T derived by the kinetic method ($r^2 = 0.99$, $P < 0.001$, n = 144) but across regions was slightly lower by an average of 7 ± 3% (repeated-measures analysis of variance, $P < 0.001$). Regional DVR, BP, and k_3/k_4 values derived by graphical method were also highly correlated with values derived with kinetic method ($r^2 = 0.99$, $P < 0.001$) but were significantly lower, by averages of 14 ± 3, 23 ± 0.10, and 28 ± 9%, for DVR, BP, and k_3/k_4, respectively.

Tables 6 and 7 display the reproducibility parameters of the graphical method. As observed for kinetic analysis, the test/retest variability of V_T (10 ± 2%) and DVR (11 ± 2%) were lower than that of BP (24 ± 7%) and k_3/k_4 (28 ± 8%). The reliability of the absolute measures (V_T ICC = 0.88 ± 0.05, BP ICC = 0.72 ± 0.17) was superior to the reliability of the relative measures (DVR ICC = 0.60 ± 0.19, k_3/k_4 ICC = 0.58 ± 0.21). The test/retest variability of all outcome measures derived with graphical analysis was higher than results of kinetic analysis (e.g., graphical BP variability = 24 ± 7%, kinetic BP variability = 14 ± 5%, paired t test, $P < 0.001$). As a consequence, the reliability of outcome measures derived with graphical analysis was lower than with the kinetic analysis (e.g., graphical BP ICC = 0.72 ± 0.17, kinetic BP ICC = 0.90 ± 0.06, paired t test, $P < 0.001$).

Noise analysis

Noise analysis was done to compare the effect of realistic noise in the images on results from the kinetic and graphical analyses (Fig. 11). A typical experiment was used to generate a simulated data set that included one cerebellar curve (two-compartment model, $K_1 = 0.120$ mL g^{-1} min^{-1}, $k_2 = 0.0526$ min^{-1}, $V_T = 2.28$ mL g^{-1}) and one caudate curve (three-compartment model, $K_1 = 0.130$ mL g^{-1} min^{-1}, $k_2 = 0.0570$ min^{-1}, $k_3 = 0.110$ min^{-1}, $k_4 = 0.034$ min^{-1}, $V_T = 9.65$ mL g^{-1}, BP = 7.38 mL g^{-1}, $k_3/k_4 = 3.24$). Random noise was then introduced as described in Materials and Methods, and noisy data sets were analyzed with kinetic and graphical analyses. Seven noise levels were investigated (SD_J of 0.04, 0.05, 0.09, 0.11, 0.13, 0.17, and 0.21), and for each noise level, 500 curves were created and analyzed. For each region and noise level, Table 8 lists the average ± SD V_T values derived with the 500 simulations, the bias (i.e., difference between average of 500 simulations and true V_T), and the error (%CV of the 500 simulations).

Both analyses were very robust as far as the cerebellum was concerned. For cerebellar kinetic analysis, the bias was negligible, and the error was very small (both bias and error < 1%). Cerebellar graphical analysis showed higher bias and errors than the kinetic analysis but remained within acceptable levels at each noise level.

TABLE 1. *Kinetic analysis of regional [^{11}C]NNC 112 uptake in human brain (three-compartment model constrained)*

Region	K_1 (mL g^{-1} min^{-1})	k_2 (min^{-1})	k_3 (min^{-1})	k_4 (min^{-1})	V_T (mL g^{-1})	BP (mL g^{-1})	DVR (unitless)	k_3/k_4 (unitless)
Caudate	0.152 ± 0.039	0.059 ± 0.008	0.132 ± 0.035	0.049 ± 0.035	10.13 ± 3.18	7.51 ± 2.98	3.89 ± 0.93	2.89 ± 0.93
Putamen	0.188 ± 0.044	0.074 ± 0.007	0.183 ± 0.083	0.057 ± 0.083	10.98 ± 2.81	8.44 ± 2.57	4.32 ± 0.80	3.32 ± 0.80
Hippocampus	0.124 ± 0.030	0.049 ± 0.007	0.015 ± 0.006	0.020 ± 0.006	4.49 ± 0.89	1.92 ± 0.77	1.77 ± 0.33	0.77 ± 0.33
Amygdala	0.112 ± 0.028	0.044 ± 0.007	0.028 ± 0.016	0.029 ± 0.016	4.90 ± 1.28	2.35 ± 1.12	1.93 ± 0.42	0.93 ± 0.42
Ant. Cingulate	0.165 ± 0.047	0.064 ± 0.011	0.037 ± 0.013	0.035 ± 0.013	5.18 ± 1.23	2.64 ± 0.98	2.04 ± 0.33	1.04 ± 0.33
DLPF Ctx	0.149 ± 0.034	0.059 ± 0.007	0.023 ± 0.007	0.030 ± 0.007	4.49 ± 1.01	1.95 ± 0.75	1.77 ± 0.27	0.77 ± 0.27
MPF Ctx	0.157 ± 0.037	0.061 ± 0.006	0.030 ± 0.007	0.033 ± 0.007	4.84 ± 1.05	2.30 ± 0.77	1.90 ± 0.26	0.90 ± 0.26
OF Ctx	0.140 ± 0.028	0.056 ± 0.010	0.028 ± 0.013	0.032 ± 0.013	4.77 ± 1.07	2.21 ± 0.97	1.89 ± 0.40	0.89 ± 0.40
Parietal Ctx	0.163 ± 0.053	0.063 ± 0.012	0.027 ± 0.010	0.032 ± 0.010	4.75 ± 1.25	2.23 ± 0.93	1.87 ± 0.31	0.87 ± 0.31
Temporal Ctx	0.139 ± 0.031	0.055 ± 0.006	0.034 ± 0.012	0.038 ± 0.012	4.86 ± 1.08	2.32 ± 0.87	1.92 ± 0.32	0.92 ± 0.32
Occipital Ctx	0.175 ± 0.044	0.069 ± 0.009	0.032 ± 0.015	0.034 ± 0.015	4.83 ± 1.09	2.29 ± 0.84	1.90 ± 0.29	0.90 ± 0.29
Thalamus	0.165 ± 0.035	0.066 ± 0.006	0.018 ± 0.005	0.032 ± 0.005	3.99 ± 0.68	1.45 ± 0.41	1.59 ± 0.16	0.59 ± 0.16
Cerebellum	0.131 ± 0.029	0.050 ± 0.008	—	—	2.54 ± 0.42	—	—	—

Values are mean ± SD of six subjects, with each value measured twice. Ant., anterior; BP, binding potential; Ctx, cortex; DLPF Ctx, dorsolateral prefrontal cortex; DVR, distribution volume ratio; MPF Ctx, medial prefrontal cortex; OF Ctx, orbitofrontal cortex

Analysis of caudate curves was more sensitive to noise. Kinetic analysis showed a small bias (+2.7% at higher noise level), and the error increased to ±14% at the highest noise level. Graphical analysis was characterized by a pronounced bias. As noise increased, graphical V_T significantly decreased, up to −38% at the highest noise level. The error on graphical V_T was comparable with that on the kinetic V_T, except that kinetic errors were larger than graphical errors at the two highest noise levels. The bias associated with graphical analysis (lower value as noise increases) was consistent with the results obtained on the experimental data set.

DISCUSSION

This study confirms the excellent imaging properties of [^{11}C]NNC 112 previously reported in two healthy volunteers (Halldin et al., 1998). In addition, model-based analysis demonstrates that kinetic analysis of brain regional uptake of [^{11}C]NNC 112 provides reliable estimates of D_1 receptor BP not only in the striatum but also in extrastriatal areas such as the limbic and neocortical regions. To our knowledge, this study represents the first demonstration of the reliability of the measurement of D_1 receptor BP in extrastriatal areas. In a recent study of the

TABLE 2. *Regional distribution of D_1 receptors in human brain:* in vitro *versus* in vivo *comparison*

	In vitro					
	Autoradiography*		Homogenate binding†		*In vivo* PET‡	
Region	Specific binding fmol/mg of tissue (Mean ± SEM) n = 4	Normalized values	Bmax pmoL g^{-1} (Mean ± SD) n = 2–6	Normalized values	BP mL g^{-1} (Mean ± SD) n = 6	Normalized values
Caudate	70.7 ± 6.2	100%	11.3 ± 3.2	100%	7.5 ± 3.0	100%
Putamen	64.7 ± 8.2	92%	9.9 ± 2.1	88%	8.4 ± 2.6	112%
Hippocampus	7.8 ± 2.0	11%	1.4 ± 0.4	12%	1.9 ± 0.8	26%
Amygdala	18.4 ± 2.7	26%	2.1 ± 1.1	19%	2.4 ± 1.1	31%
Ant. Cingulate	15.5 ± 0.9	22%	1.7 ± 0.8	15%	2.6 ± 1.0	35%
DLPF Ctx	15.2 ± 0.7	21%	3.3 ± 0.8	29%	2.0 ± 0.8	26%
OF Ctx	15.9 ± 2.4	22%	—	—	2.2 ± 1.0	29%
Parietal Ctx	18.1 ± 2.1	26%	—	—	2.2 ± 0.9	30%
Temporal Ctx	—	—	2.3 ± 0.8	20%	2.3 ± 0.9	31%
Occipital Ctx	11.4 ± 2.9	16%	—	—	2.3 ± 0.8	30%
Thalamus	4.4 ± 0.6	6%	—	—	1.5 ± 0.4	19%

Ant., anterior; BP, binding potential; Ctx, cortex; DLPF Ctx, dorsolateral prefrontal cortex; OF Ctx, orbitofrontal cortex; PET, position emission tomography.

* Specific binding of [^{3}H]SCH 23390 (1 nmol/L) in the presence of mianserin (20 nmol/L) measured with autoradiography (from De Keyser et al., 1988).

† Bmax of [^{3}H]SCH 23390 [^{3}H]SCH 23390 in the presence of ketanserin (40 nmol/L) measured in homogenated tissue (from Hall et al., 1988).

‡ BP values obtained with [^{11}C]NNC 112 imaging in 6 healthy volunteers.

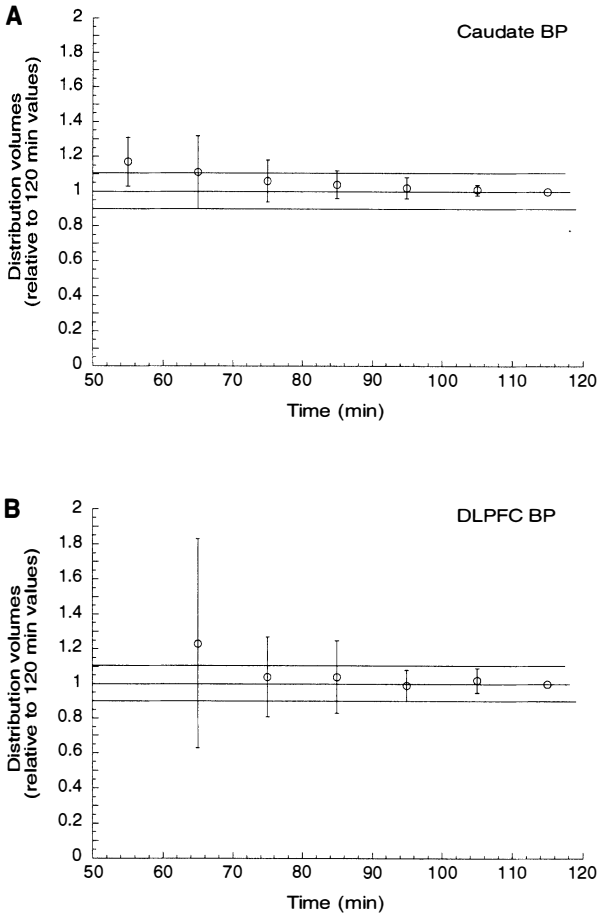

FIG. 8. Relationship between duration of data collection and kinetic derivation of binding potential (BP) in the caudate **(A)** and dorsolateral prefrontal cortex **(B)**. The BP values were normalized to the reference value; defined as the value measured with the whole data set (120 minutes of data collection). Each time point represents the mean ± SD of 12 determinations (6 subjects studied twice). For both regions, values derived after 70 minutes were within ±10% of the reference value, and the SD became low after 90 minutes. This result suggests a good stability over time of the model after 90 minutes.

reproducibility of D_1 receptor quantification with [^{11}C]SCH 23390, only measurements in the striatum were reported (Chan et al., 1998).

Comparison with [^{11}C]SCH 23390

Results of this study indicate that [^{11}C]NNC 112 achieves higher specific/nonspecific DVRs at equilibrium than [^{11}C]SCH 23390. In the putamen, [^{11}C]SCH 23390 k_3/k_4 value derived by graphical analysis was 0.85 ± 0.18 (Chan et al., 1998), lower than the value reported here with [^{11}C]NNC 112 in the same region (3.32 ± 0.80). In the PFC, Okubo et al. (1997) reported an [^{11}C]SCH 23390 k_3/k_4 value of 0.41 ± 0.06, lower than the k_3/k_4 value observed with [^{11}C]NNC 112 in the DLPFC (0.77 ± 0.33). This improvement is due not only to the higher affinity of [^{11}C]NNC 112 (K_D = 0.18 nmol/L; Andersen et al., 1992) compared with [^{11}C]SCH 23390 (0.4 nmol/L; Billard et al., 1984) but also to lower

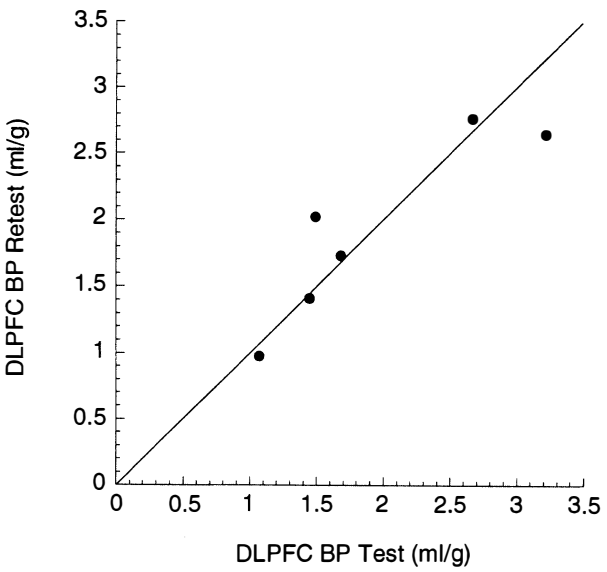

FIG. 9. Relationship between [^{11}C]NNC 112 binding potential (BP) in dorsolateral prefrontal cortex in test (x axis) and retest (y axis) conditions. The solid line represents the line of identity. Linear regression of measured values had an r^2 of 0.82, corresponding to an intraclass coefficient of 0.93.

nonspecific binding. Cerebellar V_T is 2.54 ± 0.42 mL g^{-1} for [^{11}C]NNC 112 versus 3.58 ± 0.64 mL g^{-1} for [^{11}C]SCH 23390 (Chan et al., 1998). This higher signal/noise ratio is especially valuable for quantification of D_1 receptors in the neocortex.

Neocortical region-of-interest sampling

In this study, an original method was developed for sampling of activity in neocortical regions. Measurement of activity in large subcortical regions such as the striatum is generally straightforward, inasmuch as the bound-

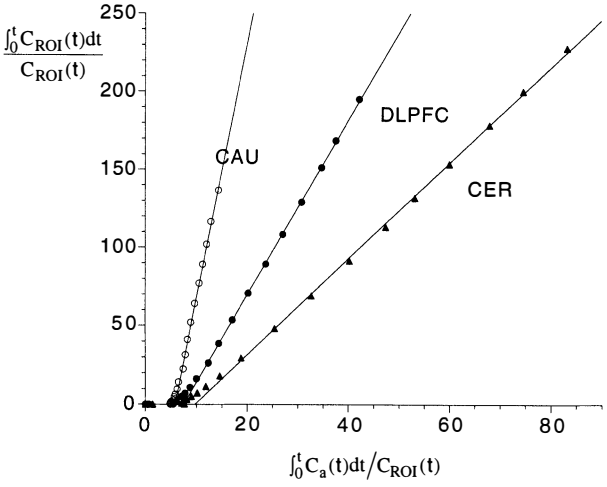

FIG. 10. Graphical analysis of [^{11}C]NNC 112 uptake in caudate (open circles), dorsolateral prefrontal cortex (filled circles), and cerebellum (triangles) after injection of 18 mCi of [^{11}C]NNC 112 (same experiment as in Fig. 6). The linearity of the relationship at normalized times of >15 min (equal to 25 minutes of real time) confirms the reversibility of the binding.

TABLE 3. *Reliability of* [^{11}C]NNC *112 distribution volume and distribution volume ratio measurements in human brain: kinetic analysis*

Measure parameter	Kinetic V_T (mL g^{-1})					Kinetic DVR (unitless)				
	Mean	BSSD (%CV)	WSSD (%CV)	VAR ± SD	ICC	Mean	BSSD (%CV)	WSSD (%CV)	VAR ± SD	ICC
Caudate	10.13	3.18 (31%)	0.41 (4%)	7% ± 02%	0.97	3.89	0.93 (24%)	0.12 (3%)	6% ± 02%	0.97
Putamen	10.98	2.81 (26%)	0.59 (5%)	10% ± 05%	0.92	4.32	0.80 (18%)	0.12 (3%)	5% ± 04%	0.96
Hippocampus	4.49	0.89 (20%)	0.32 (7%)	12% ± 12%	0.77	1.77	0.33 (19%)	0.09 (5%)	8% ± 06%	0.85
Amygdala	4.90	1.28 (26%)	0.34 (7%)	13% ± 10%	0.87	1.93	0.42 (22%)	0.12 (6%)	10% ± 08%	0.85
Ant. Cingulate	5.18	1.23 (24%)	0.26 (5%)	9% ± 09%	0.91	2.04	0.33 (16%)	0.13 (6%)	9% ± 11%	0.73
DLPF Ctx	4.49	1.01 (23%)	0.14 (3%)	6% ± 05%	0.96	1.77	0.27 (15%)	0.08 (5%)	5% ± 06%	0.82
MPF Ctx	4.84	1.05 (22%)	0.16 (3%)	6% ± 08%	0.95	1.90	0.26 (14%)	0.07 (4%)	6% ± 04%	0.87
OF Ctx	4.77	1.07 (22%)	0.26 (6%)	8% ± 09%	0.89	1.89	0.40 (21%)	0.03 (2%)	3% ± 02%	0.99
Parietal Ctx	4.75	1.25 (26%)	0.16 (3%)	7% ± 03%	0.97	1.87	0.31 (16%)	0.09 (5%)	6% ± 07%	0.83
Temporal Ctx	4.86	1.08 (22%)	0.21 (4%)	8% ± 07%	0.93	1.92	0.32 (17%)	0.11 (6%)	6% ± 08%	0.79
Occipital Ctx	4.83	1.09 (23%)	0.24 (5%)	9% ± 08%	0.91	1.90	0.29 (15%)	0.11 (6%)	7% ± 09%	0.73
Thalamus	3.99	0.68 (17%)	0.14 (3%)	7% ± 03%	0.92	1.59	0.16 (10%)	0.08 (5%)	7% ± 06%	0.69
Cerebellum	2.54	0.42 (17%)	0.09 (3%)	6% ± 06%	0.92	—	—	—	—	—
Mean ± SD				8% ± 02%	0.91 ± 0.06				6% ± 02%	0.84 ± 0.10

Ant., anterior; BSSD, between-subject SD; Ctx, cortex; DLPF Ctx, dorsolateral prefrontal cortex; DVR, distribution volume ratio; ICC, intraclass coefficient; MPF Ctx, medial prefrontal cortex; OF Ctx, orbitofrontal cortex; WSSD, within-subject SD.

aries of activity can be well defined anatomically. In the striatum, MRI-guided ROI definition does not substantially improve the reliability of the measurement compared with direct definition of the ROI on the PET image based on activity distribution (Wang et al., 1996). In contrast, measurement of activity distribution in GM cortical areas is a difficult problem due to the extent and complexity of cortical gray geometry (see discussion in Koepp et al., 1997). The simplest method is to draw geometrically simple structures (spheres, rectangles) directly on the PET scan, but this method is unreliable and influenced by the activity distribution on the PET image. Thus, defining the ROI on a coregistered MR image is preferable. However, tracing contours of a cortical region manually around the GM on high-resolution 128-slice MRI is time consuming and subject to rater bias and errors. In this study, we used a method based on coregistration of the PET data set to a segmented MRI data set, that is, a data set in which each pixel has been designated as GM, WM, or CSF value. Only the activity located in the pixels classified as GM is sampled. The advantage of constraining ROI on GM is that the segmentation procedure is operator independent and much faster and reliable than manual tracing of GM/WM/CSF boundaries. The only operator-driven choice is the choice of the limits between cortical regions, which follows well-defined criteria. The excellent reliability of the cortical measurement of [^{11}C]NNC 112 BP reported in this study indirectly supports the robustness of the method.

It is, however, important to keep in mind that this method has several limitations. Like all MRI-based ROI definitions, this method is sensitive to errors in PET-MRI coregistration. In this study, we used the minimization procedure developed by Woods et al. (1993). This pro-

TABLE 4. *Reliability of [^{11}C]NNC 112 BP and* k_3/k_4 *measurements in human brain: kinetic analysis*

Measure parameter	Kinetic BP (mL g^{-1})					Kinetic k_3/k_4 (unitless)				
	Mean	BSSD (%CV)	WSSD (%CV)	VAR ± SD	ICC	Mean	BSSD (%CV)	WSSD (%CV)	VAR ± SD	ICC
Caudate	7.51	2.98 (40%)	0.34 (5%)	8% ± 03%	0.97	2.89	0.93 (32%)	0.12 (4%)	8% ± 02%	0.97
Putamen	8.44	2.57 (30%)	0.51 (6%)	11% ± 05%	0.92	3.32	0.80 (24%)	0.12 (4%)	6% ± 05%	0.96
Hippocampus	1.92	0.77 (40%)	0.24 (13%)	18% ± 19%	0.82	0.77	0.33 (43%)	0.09 (12%)	18% ± 13%	0.85
Amygdala	2.35	1.12 (48%)	0.31 (13%)	23% ± 17%	0.86	0.93	0.42 (45%)	0.12 (13%)	21% ± 17%	0.85
Ant. Cingulate	2.64	0.98 (37%)	0.26 (10%)	19% ± 24%	0.87	1.04	0.33 (32%)	0.13 (13%)	20% ± 25%	0.73
DLPF Ctx	1.95	0.75 (39%)	0.14 (7%)	9% ± 08%	0.93	0.77	0.27 (35%)	0.08 (11%)	12% ± 11%	0.82
MPF Ctx	2.30	0.77 (34%)	0.12 (5%)	12% ± 10%	0.95	0.90	0.26 (29%)	0.07 (7%)	12% ± 08%	0.87
OF Ctx	2.21	0.97 (44%)	0.16 (7%)	11% ± 10%	0.95	0.89	0.40 (45%)	0.03 (4%)	7% ± 04%	0.99
Parietal Ctx	2.23	0.93 (42%)	0.17 (7%)	13% ± 09%	0.94	0.87	0.31 (35%)	0.09 (11%)	14% ± 12%	0.83
Temporal Ctx	2.32	0.87 (37%)	0.21 (9%)	13% ± 10%	0.89	0.92	0.32 (35%)	0.11 (12%)	11% ± 14%	0.79
Occipital Ctx	2.29	0.84 (37%)	0.23 (10%)	17% ± 12%	0.86	0.90	0.29 (32%)	0.11 (13%)	14% ± 15%	0.73
Thalamus	1.45	0.41 (28%)	0.15 (10%)	16% ± 08%	0.78	0.59	0.16 (27%)	0.08 (13%)	18% ± 12%	0.63
Mean ± SD				14% ± 05%	0.90 ± 0.06				13% ± 05%	0.84 ± 0.11

Ant., anterior; BP, binding potential; BSSD, between-subject SD; Ctx, cortex; DLPF Ctx, dorsolateral prefrontal cortex; ICC, intraclass coefficient; MPF Ctx, medial prefrontal cortex; OF Ctx, orbitofrontal cortex; WSSD, within-subject SD.

TABLE 5. *Graphical analysis of regional [^{11}C]NNC 112 uptake in human brain*

Region	V_T (mL g^{-1})	BP (mL g^{-1})	DVR (unitless)	k_3/k_4 (unitless)
Caudate	9.20 ± 3.25	6.45 ± 3.03	3.34 ± 0.91	2.34 ± 0.91
Putamen	10.57 ± 2.92	7.82 ± 2.65	3.84 ± 0.77	2.84 ± 0.77
Hippocampus	3.85 ± 0.78	1.15 ± 0.47	1.41 ± 0.22	0.43 ± 0.18
Amygdala	4.51 ± 1.18	1.75 ± 0.97	1.65 ± 0.34	0.65 ± 0.34
Ant. Cingulate	4.94 ± 1.22	2.19 ± 0.92	1.80 ± 0.28	0.80 ± 0.28
DLPF Ctx	4.19 ± 1.01	1.43 ± 0.72	1.52 ± 0.24	0.52 ± 0.24
MPF Ctx	4.59 ± 1.06	1.84 ± 0.73	1.67 ± 0.22	0.67 ± 0.22
OF Ctx	4.38 ± 1.22	1.71 ± 1.05	1.61 ± 0.41	0.67 ± 0.38
Parietal Ctx	4.43 ± 1.32	1.75 ± 0.84	1.59 ± 0.30	0.63 ± 0.25
Temporal Ctx	4.66 ± 1.09	1.90 ± 0.84	1.70 ± 0.28	0.70 ± 0.28
Occipital Ctx	4.62 ± 1.13	1.86 ± 0.84	1.68 ± 0.26	0.68 ± 0.26
Thalamus	3.56 ± 0.81	0.84 ± 0.48	1.30 ± 0.19	0.31 ± 0.17
Cerebellum	2.75 ± 0.48	—	—	—

Values are mean ± SD of six subjects, with each value measured twice. Ant., anterior; BP, binding potential; Ctx, cortex; DLPF, dorsolateral prefrontal cortex; DVR, distribution volume ratio; MPF Ctx, medial prefrontal cortex; OF Ctx, orbitofrontal cortex.

cedure has a reported average three-dimensional error of <2 mm for between-modality registration, which is acceptable, given a camera resolution of 6 mm. Second, this sampling method results in inherent subsampling, inasmuch as the activity spilling over the WM is not measured. This subsampling is desirable from an accuracy point of view but results in a loss of information that might translate into increased noise. Finally, this method does not correct for partial voluming, which is considerable in the cortex. Yet, it provides a necessary first step for implementation of ROI-based partial volume correction (Rousset et al., 1998). In fact, partial volume correction would result in a recovery of the spilled-over information. Thus, partial volume correction has the potential not only to increase the accuracy of the measurement but also to reduce the error by using the information that is rejected in the present method. We are currently developing and testing a partial volume correction method that would address these issues.

Evaluation of kinetic approach

Evaluation of model-based methods for quantification of receptor parameters includes assessment of various criteria, namely, identifiability, validity, stability, and reliability. The identifiability is a mathematical dimension referring to the confidence in the value of the parameter as derived by the fitting process. The validity refers to the physiological plausibility of the parameters and is usually determined in relationship to *in vitro* results. The stability refers to the independence of the parameter estimate from the amount of data collected, in this case the duration of the experiment. The reliability expresses the test/retest variability in relation to between-subject differences. Kinetic analysis of [^{11}C]NNC 112 regional uptake performed well on all of these criteria.

Kinetic analysis of the cerebellum presented an interesting problem. The three-compartment model provided a slightly but significantly superior fit to the data compared with the two-compartment model. The observation of a better fit by the three- compared with the two-compartment model for a region of a reference is the rule rather than the exception in neuroreceptor imaging (Frost et al., 1989; Logan et al., 1990; Laruelle et al., 1994*b*,*c*; Lammertsma et al., 1996; Abi-Dargham et al., 1997; Ito et al., 1998). The absence of specific binding in the cerebellum is confirmed by the absence of displacement of [^{11}C]NNC 112 uptake in the cerebellum after injection of SCH 23390 (2.5 mg/kg) (Halldin et al., 1998). Thus, the small second tissue compartment revealed by the three-compartment model's superior fit might reflect a slow buildup of radiolabeled metabolites in the brain or the existence of a nonspecific binding component with slow

TABLE 6. *Reliability of [^{11}C]NNC 112 distribution volumes and distribution volume ratio measurements in human brain: graphical analysis*

	Graphical V_T (mL g^{-1})					Graphical DVR (unitless)				
Measure parameter	Mean	BSSD (%CV)	WSSD (%CV)	VAR ± SD	ICC	Mean	BSSD (%CV)	WSSD (%CV)	VAR ± SD	ICC
Caudate	9.20	3.25 (35%)	0.60 (7%)	11% ± 08%	0.93	3.34	0.91 (27%)	0.19 (6%)	11% ± 04%	0.92
Putamen	10.57	2.92 (28%)	0.90 (9%)	14% ± 11%	0.83	3.84	0.77 (20%)	0.23 (6%)	11% ± 09%	0.83
Hippocampus	3.85	0.78 (20%)	0.27 (7%)	11% ± 10%	0.78	1.41	0.22 (15%)	0.14 (10%)	13% ± 14%	0.41
Amygdala	4.51	1.18 (26%)	0.24 (5%)	10% ± 06%	0.92	1.65	0.34 (20%)	0.13 (8%)	12% ± 11%	0.74
Ant. Cingulate	4.94	1.22 (25%)	0.35 (7%)	12% ± 09%	0.85	1.80	0.28 (15%)	0.17 (9%)	13% ± 14%	0.46
DLPF Ctx	4.19	1.01 (24%)	0.20 (5%)	8% ± 05%	0.92	1.52	0.24 (16%)	0.12 (8%)	10% ± 10%	0.58
MPF Ctx	4.59	1.06 (23%)	0.19 (4%)	8% ± 04%	0.94	1.67	0.22 (13%)	0.10 (6%)	10% ± 06%	0.63
OF Ctx	4.38	1.22 (28%)	0.21 (5%)	10% ± 06%	0.94	1.61	0.41 (25%)	0.09 (5%)	10% ± 09%	0.92
Parietal Ctx	4.43	1.32 (30%)	0.30 (7%)	12% ± 09%	0.90	1.59	0.30 (19%)	0.17 (11%)	15% ± 17%	0.50
Temporal Ctx	4.66	1.09 (23%)	0.25 (5%)	8% ± 07%	0.90	1.70	0.28 (17%)	0.13 (8%)	8% ± 11%	0.64
Occipital Ctx	4.62	1.13 (25%)	0.32 (7%)	11% ± 08%	0.85	1.68	0.26 (16%)	0.16 (10%)	11% ± 14%	0.45
Thalamus	3.56	0.81 (23%)	0.25 (7%)	10% ± 09%	0.83	1.30	0.19 (15%)	0.13 (10%)	12% ± 14%	0.38
Cerebellum	2.75	0.48 (17%)	0.11 (4%)	7% ± 06%	0.89	—	—	—	—	—
Mean ± SD				10% ± 02%	0.88 ± 0.05				11% ± 02%	0.60 ± 0.19

Ant., anterior; BSSD, between-subject SD; Ctx, cortex; DLPF Ctx, dorsolateral prefrontal cortex; DVR, distribution volume ratio; ICC, intraclass coefficient; MPF Ctx, medial prefrontal cortex; OF Ctx, orbitofrontal cortex; WSSD, within-subject SD.

TABLE 7. *Reliability of [^{11}C]NNC 112 BP and k_3/k_4 measurements in human brain: graphical analysis*

Measure parameter	Graphical BP (mL g^{-1})					Graphical k_3/k_4 (unitless)				
	Mean	BSSD (%CV)	WSSD (%CV)	VAR ± SD	ICC	Mean	BSSD (%CV)	WSSD (%CV)	VAR ± SD	ICC
Caudate	6.45	3.03 (47%)	0.55 (8%)	14% ± 12%	0.94	2.34	0.91 (39%)	0.19 (8%)	16% ± 07%	0.92
Putamen	7.82	2.65 (34%)	0.83 (11%)	17% ± 16%	0.82	2.84	0.77 (27%)	0.23 (8%)	16% ± 13%	0.83
Hippocampus	1.15	0.47 (41%)	0.32 (27%)	27% ± 32%	0.38	0.43	0.18 (42%)	0.13 (30%)	30% ± 37%	0.32
Amygdala	1.75	0.97 (55%)	0.31 (18%)	41% ± 39%	0.82	0.65	0.34 (52%)	0.13 (20%)	43% ± 43%	0.74
Ant. Cingulate	2.19	0.92 (42%)	0.40 (18%)	28% ± 35%	0.69	0.80	0.28 (35%)	0.17 (21%)	33% ± 35%	0.46
DLPF Ctx	1.43	0.72 (50%)	0.27 (19%)	24% ± 17%	0.76	0.52	0.24 (45%)	0.12 (23%)	30% ± 20%	0.58
MPF Ctx	1.84	0.73 (40%)	0.22 (12%)	21% ± 14%	0.83	0.67	0.22 (33%)	0.10 (16%)	26% ± 13%	0.63
OF Ctx	1.71	1.05 (61%)	0.12 (7%)	16% ± 17%	0.98	0.67	0.38 (56%)	0.06 (9%)	34% ± 35%	0.95
Parietal Ctx	1.75	0.84 (48%)	0.34 (19%)	22% ± 23%	0.72	0.63	0.25 (39%)	0.14 (23%)	22% ± 29%	0.49
Temporal Ctx	1.90	0.84 (44%)	0.29 (15%)	19% ± 16%	0.78	0.70	0.28 (40%)	0.13 (19%)	20% ± 22%	0.64
Occipital Ctx	1.86	0.84 (45%)	0.38 (21%)	24% ± 22%	0.66	0.68	0.26 (39%)	0.16 (24%)	25% ± 28%	0.45
Thalamus	0.84	0.48 (57%)	0.30 (35%)	26% ± 37%	0.45	0.31	0.17 (54%)	0.12 (40%)	32% ± 40%	0.29
Mean ± SD				24% ± 07%	0.72 ± 0.17				28% ± 08%	0.58 ± 0.21

Ant., anterior; BP, binding potential; BSSD, between-subject SD; Ctx, cortex; DLPF Ctx, dorsolateral prefrontal cortex; ICC, intraclass coefficient; MPF Ctx, medial prefrontal cortex; OF Ctx, orbitofrontal cortex; WSSD, within-subject SD.

kinetics. The presence of a statistically superior fit with the three-compartment model would usually suggest the use of a three-compartment model to derive cerebellar V_T. However, in this case, V_T derived by the three-compartment model was less well identified than with a two-compartment model, was markedly affected by the duration of the scan, had a poor test/retest reproducibility (negative ICC), and provided values much larger than the value of V_T derived by the graphical analysis. Thus, whereas the goodness of fit favored the three-compartment model, all other criteria favored the two-compartment model. For these reasons, we favored the two-compartment model, that is, the solution that provides superior identifiability, stability, validity, and reproducibility.

For ROIs, we used a three-compartment model with K_1/k_2 ratio constrained to the value of V_T measured in the cerebellum. Whereas an unconstrained three-compartment model is usually appropriate to derive V_T, the separate derivation of V_2 and BP is not reliable with an unconstrained three-compartment model (Laruelle et al., 1994*d*,*e*; Lammertsma et al., 1996). The constrained approach takes advantage of the knowledge of V_2 derived from the region of reference while accommodating regional differences in blood flow. The validity of this approach is supported by the homogeneous distribution of the inactive enantiomer (−)[^{11}C]NNC 112 within the human and baboon brain (Halldin et al., 1998). The goodness of fit was excellent, with even distribution of the residuals, and regional distribution volumes were well identified.

A significant relationship was observed between regional BP and regional density of D_1 receptor measured *in vitro* in the human brain (Table 2). Yet, subtle differences were observed. *In vitro,* D_1 receptor density is slightly higher in caudate than putamen, whereas the reverse is true in the PET measurements. *In vitro,* D_1 receptor density is higher in the amygdala than hippocampus, but this difference is less pronounced in the PET measurements. *In vitro,* frontal D_1 receptor density is higher than occipital D_1 receptor density, but PET measurements gave similar BP. These differences can be accounted for by partial volume effects, resulting in relative underestimation of smaller regions versus larger regions (caudate versus putamen, amygdala versus hippocampus, frontal GM versus occipital GM).

Results of kinetic modeling were essentially stable from 90 minutes to the end of the experiment. The stability over time of the solution means that the model describes the data appropriately and that enough data were collected to inform the model. Remarkably, this was true for both striatal and extrastriatal areas. It is often difficult to accurately measure receptor parameters with the same radiotracer both in regions with high and low receptor densities. High affinity is required for a high signal/noise ratio in regions with low receptor density, but high affinity might preclude favorable kinetics in regions with high receptor density. [^{11}C]NNC 112 achieves an effective balance between these competing requirements. However, 90 minutes of data was needed to achieve stability of the outcome measure. The three-dimensional acquisition mode, with its higher sensitivity, is crucial to enable data collection up to 120 minutes. The use of the polyurethane head mold was effective, as only minimal head movement was recorded during this prolonged time frame. Head movement was measured by comparing the spatial location of the ^{11}C markers on each frame and was <2.5 mm per frame in ~90% of the cases. Thus, the combination of the high sensitivity of the three-dimensional mode and the effective headholder allowed collection of enough data to achieve stability of the results.

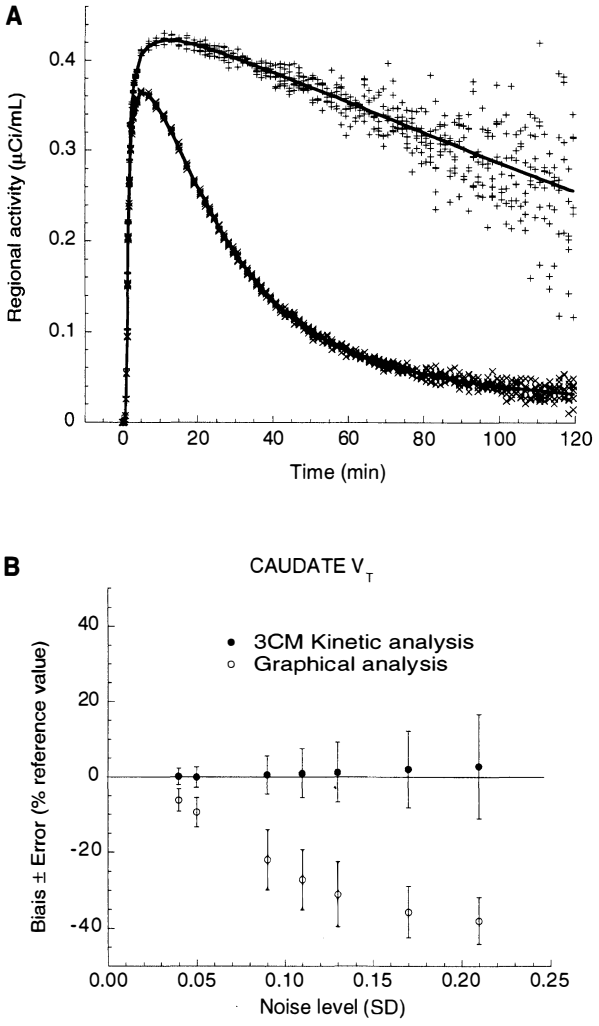

FIG. 11. Noise analysis. **(A)** Simulated time–activity data in caudate and cerebellum. The solid line represents a simulated noise-free brain response to a typical input function with a typical set of kinetic parameters. Crosses correspond to 10 simulated brain responses with random noise. Noise had 0 mean and a SD (SD_J) of 0.09. The noise increases with the duration of the experiment to reflect the decay of ^{11}C. **(B)** Results of analysis of caudate data sets with random noise, at different noise levels corresponding to SN_J ranging from low (0.04) to high noise (0.21). At each level, 10 curves were generated and analyzed with kinetic and graphical analyses. Values correspond to the mean V_T values of these 10 analyses, expressed as relative difference from the true value used to generate the simulation. The vertical bar is the SD of the result from the 10 simulations. For kinetic analysis, no significant bias is observed; that is, the mean of 10 simulations is close to the true value. In contrast, graphical analysis is affected by a noise-dependent bias. As the noise increases, the mean V_T value derived from the 10 simulations becomes lower than the true value. The SD of the 10 V_T values increased as the noise level increased similarly for kinetic and graphical analyses.

Reproducibility and outcome measures

Several statistical parameters and outcome measures are used in the PET/single photon emission computed tomography neuroreceptor literature to report the reproducibility of the measurements. The most straightforward reproducibility parameter is the absolute test/retest variability, calculated as the absolute difference between test and retest values divided by their average (Abi-Dargham et al., 1995; Seibyl et al., 1995; Smith et al., 1998). A second method consists of reporting the within-subject SD (or %CV) of the measurement (Chan et al., 1998). When the number of repeat scans is 2, the within-subject %CV is smaller than the variability by a factor of $2^{1/2}$. Finally, the ICC provides a measure of the reproducibility of the measurement relative to between-subject differences and is the most useful measure to compare results of various methods.

In this study, four outcome measures (V_T, DVR, BP, and k_3/k_4) were compared in terms of reproducibility and reliability. These commonly used outcome measures in the PET literature have very different relationships vis à vis receptor B_{max} and K_D. In essence, V_T and BP are "absolute" measures that relate brain distribution volumes to the input function and are expressed as milliliters (of plasma) over grams (of tissue). V_T is the total distribution volume, including free, nonspecific, and specific binding. The use of V_T as outcome measure should be restricted to situations when nonspecific binding cannot be measured for a lack of region of reference and is negligible compared with the specific binding, such as in the case of [^{11}C]flumazenil (Koeppe et al., 1991) or [^{123}I]iomazenil (Abi-Dargham et al., 1994). Otherwise, BP is the outcome measure of choice because it is directly equal to the B_{max}/K_D ratio and does not include nonspecific binding. The reproducibility of V_T is intrinsically superior to BP, as BP is derived by the difference between two V_T measurements (V_T of the ROI and V_T of the region of reference), and this is especially true in regions with low BP relative to V_2. In this study, the test/retest variability of V_T (8 ± 2%) was better than the variability of BP (14 ± 5%).

In contrast to V_T and BP, DVR and k_3/k_4 are "relative" outcome measures in the sense that they represent distribution volumes "normalized" by the region of reference, in this case the cerebellum. Both outcome measures are related (DVR − 1 = k_3/k_4), yet only k_3/k_4 expresses a meaningful quantity. Although both outcome measures are linearly related to BP, the relationship between DVR and BP has an intercept of 1, meaning that DVR assumes a value of 1 in a region with BP = 0. Thus, DVR is inappropriate to express receptor density. However, studies reporting reproducibility of neuroreceptor measurements frequently report DVR instead of k_3/k_4 (Volkow et al., 1993; Chan et al., 1998; Smith et al., 1998). The reproducibility of DVR is intrinsically better than the reproducibility of k_3/k_4, and this is especially true in regions with low receptor density. In this study, the test/retest variabilities of DVR and k_3/k_4 were 6 ± 2 and 13 ± 5%, respectively. The DVR variability observed in this study (6%) is in the same range as the variability of DVR for [^{11}C]raclopride in the striatum

TABLE 8. *Noise analysis of cerebellum and caudate: comparison of kinetic and graphical methods*

Region noise level (SDJ)	Cerebellum					
	Kinetic analysis (2CM)			Graphical analysis		
	$V_T \pm SD$	Bias	Error	$V_T \pm SD$	Bias	Error
0	2.3085			2.2156	—	—
0.04	2.3086 ± 0.0031	0.00%	0.13%	2.2078 ± 0.0073	−0.35%	0.33%
0.05*	2.3083 ± 0.0038	−0.01%	0.16%	2.2031 ± 0.0099	−0.56%	0.45%
0.09	2.3087 ± 0.0069	0.01%	0.30%	2.1723 ± 0.0250	−1.95%	1.15%
0.11	2.3088 ± 0.0085	0.01%	0.37%	2.1561 ± 0.0291	−2.69%	1.35%
0.13	2.3084 ± 0.0098	0.00%	0.42%	2.1405 ± 0.0332	−3.39%	1.55%
0.17	2.3091 ± 0.0131	0.03%	0.57%	2.1178 ± 0.0316	−4.41%	1.49%
0.21	2.3075 ± 0.0166	−0.04%	0.72%	2.1093 ± 0.0321	−4.80%	1.52%
	Caudate					
	Kinetic analysis (3CMcst)			Graphical analysis		
0	9.6594	—	—	9.6216	—	—
0.04	9.6726 ± 0.2129	0.14%	2.20%	9.0261 ± 0.2679	−6.19%	2.97%
0.05*	9.6575 ± 0.2637	−0.02%	2.73%	8.7161 ± 0.3426	−9.41%	3.93%
0.09	9.7159 ± 0.4899	0.58%	5.04%	7.4942 ± 0.5946	−22.11%	7.93%
0.11	9.7549 ± 0.6340	0.99%	6.50%	6.9921 ± 0.5585	−27.33%	7.99%
0.13	9.7813 ± 0.7817	1.26%	7.99%	6.6233 ± 0.5671	−31.16%	8.56%
0.17	9.8543 ± 1.0004	2.02%	10.15%	6.1875 ± 0.4183	−35.69%	6.76%
0.21	9.9252 ± 1.3677	2.75%	13.78%	5.9661 ± 0.3705	−37.99%	6.21%

* Noise level observed in experimental data set.

(5%) (Volkow et al., 1993), [^{11}C]SCH 23390 in the striatum (within-subject %CV of 3%) (Chan et al., 1998), and [^{18}F]altanserin in cortical regions (ranging from 7 to 9%, n = 8) (Smith et al., 1998).

BP versus k_3/k_4

As a region of reference can be measured for [^{11}C]NNC 112 (i.e., cerebellum), the only meaningful choices of outcome measures for clinical studies are either BP or k_3/k_4. Usually, the reproducibility of k_3/k_4 is better than BP because the data are normalized by cerebellum V_T and k_3/k_4 is less sensitive to errors associated with plasma input function measurement and cross-calibration between PET camera and well counter. However, in this study, the average test/retest variability of BP (14 ± 5%) was similar to that of k_3/k_4 (13 ± 5%), and the reliability of BP (ICC = 0.90 ± 0.06) was slightly better than that of k_3/k_4 (0.84 ± 0.11). Thus, according to these data, both outcome measures essentially perform similarly, and the choice between the two depends on the inherent assumptions one is willing to accept.

The BP as expressed in Eq. 10 is the only expression of BP that is exclusively dependent on receptor parameters and unbiased by factors unrelated to receptors. However, in this study, BP was not corrected for f_1. The free fraction of [^{11}C]NNC 112 in plasma was low (1.02 ± 0.28% of total plasma concentration), and no between-subject differences in f_1 were reliably detected (f_1 ICC = −0.20). Thus, the within-subject %CV associated with f_1 measurement (±34%) was of the same magnitude as the between-subject %CV in f_1 (±27%). Under these conditions, individual f_1 values should not be used in the calculation of the distribution volumes (Abi-Dargham et al., 1995). Yet, the use of this uncorrected BP is associated with a potential bias introduced by between-subject differences in f_1. Although this study did not support the utility of this correction in healthy subjects, it may still be necessary to control for potential alterations of plasma protein binding in pathological conditions. On the other hand, the cost associated with the use of k_3/k_4 is the potential bias introduced by between-subject differences in nonspecific binding, which might lead to between-subject differences in k_3/k_4 that are unrelated to receptor parameters. True between-subject differences in nonspecific binding were demonstrated in this study (the between-subject %CV of cerebellum V_T was 17%). Thus, both the uncorrected BP used in this study and k_3/k_4 have potential pitfalls. Between-subject differences in plasma protein binding would bias BP but not k_3/k_4. Between-subject differences in nonspecific binding to brain tissue would bias k_3/k_4 but not BP. With these limitations in mind, the slightly better reliability of BP compared with k_3/k_4 suggests that BP should be the outcome measure of choice for between-subject comparison. Yet, this advantage might be offset by the convenience of measuring k_3/k_4 using the cerebellum as input function instead of the plasma (Ichise et al., 1996; Lammertsma et al., 1996; Logan et al., 1996). Additional analysis comparing the reliability of k_3/k_4 measurement with and without plasma input function is required to resolve this issue.

Kinetic versus graphical analysis

Distribution volumes derived by graphical and kinetic analyses were strongly correlated ($r^2 = 0.99$, $P < 0.001$),

but results of graphical analysis resulted in lower values of V_T (by 7 ± 3%), BP (by 23 ± 10%), and k_3/k_4 (28 ± 9%). Differences between graphical and kinetic BP and k_3/k_4 can be partially accounted for by the fact that cerebellum V_T was higher with graphical than kinetic analysis, which might be linked to an underestimation of cerebellum V_T as derived by two-compartment model. However, these differences are also due to differences in ROI V_T. A systematic difference between kinetic and graphical V_T was an unexpected finding. Another unexpected difference was the lower reproducibility of graphical V_T (test/retest variability = 10 ± 2%, ICC = 0.88) compared with kinetic V_T (8 ± 2%, ICC = 0.91). The lower reproducibility of graphical compared with kinetic outcomes was even more accentuated for BP and k_3/k_4. This result undermines the claim that graphical analysis is less sensitive to noise and statistical fluctuation of the data than kinetic analysis (Volkow et al., 1993).

Analysis of the effect of noise on the outcome measure derived by both methods was performed to better understand this phenomenon. Realistic noisy data sets were generated in which the noise increased with the duration of the experiment proportionally to the decay of ^{11}C. The impact of the noise on the outcome measure was very different for kinetic and graphical analyses. As noise increased, both methods were associated with a similar variability, but V_T derived by kinetic analysis remained essentially unbiased, whereas the graphical analysis yielded systematically lower values. As the noise was randomly distributed around the true values with zero mean, the noise-introduced bias toward lower outcome measures in the graphical analysis was not intuitively predicted. This noise-dependent bias was introduced by the linearization process in which both predictor and response variables are subject to error. This phenomenon, observed here for the graphical analysis, is comparable with the noise-dependent bias introduced by the Scatchard transformation used in analysis of saturation binding data (Munson and Rodbard, 1980) and has been previously described (Carson, 1993).

At the highest noise level (SD_J = 0.21), this bias resulted in a 38% underestimation of V_T by graphical analysis (i.e., the mean of the 500 simulations was 38% lower than the true value used to generate the curves). Simulations performed on other regions such as the DLPFC yielded similar results (data not shown). We also observed that the noise-dependent bias was related to the slope of the regression (i.e., on the magnitude of V_T). Therefore, regions with lower receptor density were less vulnerable to this effect than regions with high receptor density (cerebellum < DLPFC < caudate). This slope dependency also contributed to the greater underestimation of BP and k_3/k_4 by graphical analysis compared with V_T, to the extent that regions with receptors were more affected than cerebellum.

A large range of noise was used to generate these simulations (SD_J from 0.04 to 0.21). To determine which level of noise corresponded to the experimental noise, we compared the mean sum of squares of the residuals as well as the identifiability (percent error) of V_T at each level of noise in the simulations with the mean sum of squares and percent error effectively observed in the experimental data set. The mean sum of squares observed in the caudate in the experimental data was 0.35 ± 0.21 nCi/mL (n = 12). The simulations with SD_J of 0.04 and 0.05 gave mean mean sums of squares of 0.25 and 0.39 nCi/mL, respectively. The percent error associated with V_T in the caudate in the experimental data was 2.6 ± 0.7% (n = 12). The simulations with SD_J of 0.05 and 0.09 had percent errors of 1.8 and 3.2%, respectively. Thus, the experimental mean sum of squares falls between SD_J of 0.04 and 0.05, and the experimental percent error falls between SD_J of 0.05 and 0.09. Therefore, the simulation with SD_J of 0.05 appears to provide a noise level comparable with the noise observed experimentally.

At this noise level, caudate kinetic analysis had no bias (−0.02%), but the graphical analysis had a significant bias (−9.41%). The bias associated with graphical analysis at this noise level might account for the lower V_T measured in the caudate with the graphical analysis (9.3 ± 3.6 mL g^{-1}) compared with the kinetic analysis (10.3 ± 3.6 mL g^{-1}). This difference was significant (repeated-measures analysis of variance, P = 0.007) and averaged −11 ± 7%. In addition, as the noise might vary from test to retest condition, this phenomenon might explain the lower reproducibility of the graphical method compared with the kinetic analysis. These results indicate that kinetic modeling is the method of choice for the derivation of D_1 receptor BP or k_3/k_4 with [^{11}C]NNC 112.

CONCLUSION

This study confirms that [^{11}C]NNC 112 is a superior radiotracer with which to measure D_1 receptors in both the striatal and the extrastriatal areas. The main limitation of this radiotracer is that 90 minutes of data collection is needed to yield stable outcome measures. Simplified approaches that do not require input function measurement still need to be evaluated. Because it allows reliable estimation of D_1 receptor parameters in extrastriatal areas, [^{11}C]NNC 112 might play an important role in elucidating the role of D_1 receptors in cognition in health and disease and in psychopathology.

Acknowledgments: The authors thank Suehee Chung, Bryan Bergert, Ann Shinn, Alexei Kartachov, Richard Weiss, Analia Arevaldo, Julie Montoya, Daniel Schneider, and the technologists of the Columbia PET Center for excellent technical assistance.

REFERENCES

Abi-Dargham A, Laruelle M, Seibyl J, Rattner Z, Baldwin RM, Zoghbi SS, Zea-Ponce Y, Bremner JD, Hyde TM, Charney DS, Hoffer PB, Innis RB (1994) SPECT measurement of benzodiazepine receptors in human brain with [^{123}I]iomazenil: kinetic and equilibrium paradigms. *J Nucl Med* 35:228–238

Abi-Dargham A, Gandelman M, Zoghbi SS, Laruelle M, Baldwin RM, Randall P, Zeaponce Y, Charney DS, Hoffer PB, Innis RB (1995) Reproducibility of SPECT measurement of benzodiazepine receptors in human brain with iodine-123-iomazenil. *J Nucl Med* 36: 167–175

Abi-Dargham A, Zea-Ponce Y, Terriere D, Al-Tikriti M, Baldwin R, Hoffer P, Charney D, Leysen JE, Laruelle M, Mertens J, Innis RB (1997) Preclinical evaluation of [I-123]R93274 as a SPECT radiotracer for imaging serotonin 5-HT2A receptors. *Eur J Pharmacol* 321:285–293

Abi-Dargham A, Simpson N, Kegeles L, Parsey R, Hwang DR, Anjilvel S, Zea-Ponce Y, Lombardo I, Van Heertum R, Mann JJ, Foged C, Halldin C, Laruelle M (1999) PET studies of binding competition between endogenous dopamine and the D1 radiotracer [^{11}C]NNC 756. *Synapse* 32:93–109

Akaike H (1974) A new look at the statistical model identification. *IEEE Trans Automat Contr* AC19:716–723

Andersen PH, Gronvald FC, Hohlweg R, Hansen LB, Guddal E, Braestrup C, Nielsen EB (1992) NNC-112, NNC-687 and NNC-756, new selective and highly potent dopamine D1 receptor antagonists. *Eur J Pharmacol* 219:45–52

Arnsten AF, Cai JX, Murphy BL, Goldman-Rakic PS (1994) Dopamine D1 receptor mechanisms in the cognitive performance of young adult and aged monkeys. *Psychopharmacology* 116:143–151

Bernabeu R, Bevilaqua L, Ardenghi P, Bromberg E, Schmitz P, Bianchin M, Izquierdo I, Medina JH (1997) Involvement of hippocampal cAMP/cAMP-dependent protein kinase signaling pathways in a late memory consolidation phase of aversively motivated learning in rats. *Proc Natl Acad Sci USA* 94:7041–7046

Billard W, Ruperto V, Crosby G, Iorio LC, Barnett A (1984) Characterization of the binding of ^{3}H-SCH 23390, a selective D-1 receptor antagonist ligand, in rat striatum. *Life Sci* 35:1885–1893

Burger C, Buck A (1997) Requirements and implementation of a flexible kinetic modeling tool. *J Nucl Med* 38:1818–1823

Carson RE (1986) Parameters estimation in positron emission tomography. In: *Positron emission tomography. Principles and applications for the brain and the heart* (Phelps ME, Mazziotta JC, Schelbert HR, eds), New York: Raven Press, pp 347–390

Carson RE (1993) PET parameter estimation using linear integration methods: bias and variability. In: *Quantification of brain function. Tracer kinetic and image analysis in brain PET* (Uemura K, Lassen NA, Jones T, Kanno I, eds), New York: Elsevier Science, pp 499–507

Chan GL, Holden JE, Stoessl AJ, Doudet DJ, Wang Y, Dobko T, Morrison KS, Huser JM, English C, Legg B, Schulzer M, Calne DB, Ruth TJ (1998) Reproducibility of the distribution of carbon-11-SCH 23390, a dopamine D1 receptor tracer, in normal subjects. *J Nucl Med* 39:792–797

De Keyser J, Claeys A, De Backer JP, Ebinger G, Roels F, Vauquelin G (1988) Autoradiographical localization of D1 and D2 dopamine receptors in the human brain. *Neurosci Lett* 91:142–147

Duvernoy H (1991) *The human brain. Surface, three-dimensional sectional anatomy and MRI*. New York: Springer-Verlag

Farde L, Halldin C, Stone-Elander S, Sedvall G (1987) PET analysis of human dopamine receptors subtypes using ^{11}C-SCH 23390 and ^{11}C-raclopride. *Psychopharmacology* 92:278–284

Frost JJ, Douglass KH, Mayberg HS, Dannals RF, Links TM, Wilson AA, Ravert HT, Crozier WC, Wagner HNJ (1989) Multicompartmental analysis of ^{11}C-carfentanil binding to opiate receptors in human measured by positron emission tomography. *J Cereb Blood Flow Metab* 9:398–409

Gandelman MS, Baldwin RM, Zoghbi SS, Zea-Ponce Y, Innis RB (1994) Evaluation of ultrafiltration for the free fraction determination of single photon emission computerized tomography (SPECT) radiotracers: β-CIT, IBF and iomazenil. *J Pharm Sci* 83:1014–1019

Gjedde A, Wong DF (1990) Modeling neuroreceptor binding of radioligands in vivo. In: *Quantitative imaging: neuroreceptors, neurotransmitters, and enzymes* (Frost JJ, Wagner HN Jr, eds), New York: Raven Press, pp 51–79

Graham MM, Lewellen BL (1993) High-speed automated discrete blood sampling for positron emission tomography. *J Nucl Med* 34:1357–1360

Hall H, Farde L, Sedvall G (1988) Human dopamine receptors subtypes—in vitro binding analysis using [^{3}H]SCH 23390 and [^{3}H]raclopride. *J Neural Transm* 73:7–21

Hall H, Sedvall G, Magnusson O, Kopp J, Halldin C, Farde L (1994) Distribution of D1- and D2-dopamine receptors, and dopamine and its metabolites in the human brain. *Neuropsychopharmacology* 11: 245–256

Halldin C, Stone-Elander S, Farde L, Ehrin E, Fasth KJ, Langström B, Sedvall G (1986) Preparation of ^{11}C-labelled SCH 23390 for the in vivo study of dopamine D1 receptors using positron emission tomography. *Appl Radiat Isot* 37:1039–1043

Halldin C, Foged C, Farde L, Karlsson P, Hansen K, Gornvald F, Swahn C-G, Hall H, Sedvall G (1993) [^{11}C]NNC 687 and [^{11}C]NNC 756, dopamine D-1 receptor ligands. Preparation, autoradiography and PET investigation in monkey. *Nucl Med Biol* 8:945–953

Halldin C, Foged C, Chou YH, Karlsson P, Swahn CG, Sandell J, Sedvall G, Farde L (1998) Carbon-11-NNC 112: a radioligand for PET examination of striatal and neocortical D1-dopamine receptors. *J Nucl Med* 39:2061–2068

Huang YY, Kandel ER (1995) D1/D5 receptor agonists induce a protein synthesis-dependent late potentiation in the CA1 region of the hippocampus. *Proc Natl Acad Sci USA* 92:2446–2450

Ichise M, Ballinger JR, Golan H, Vines D, Luong A, Tsai S, Kung HF (1996) Noninvasive quantification of dopamine D2 receptors with iodine-123-IBF SPECT. *J Nucl Med* 37:513–520

Ito H, Nyberg S, Halldin C, Lundvist C, Farde L (1998) PET imaging of central 5-HT2A receptors with carbon-11-MDL 100,907. *J Nucl Med* 39:208–214

Karlsson P, Farde L, Halldin C, Swahn CG, Sedvall G, Foged C, Hansen KT, Skrumsager B (1993) PET examination of [^{11}C]NNC 687 and [^{11}C]NNC 756 as new radioligands for the D1-dopamine receptor. *Psychopharmacology* 113:149–156

Karlsson P, Farde L, Halldin C, Sedvall G (1997) D1-Dopamine receptors in schizophrenia examined by PET. *Schizophr Res* 24:179

Kates WR, Abrams MT, Kaufmann WE, Breiter SN, Reiss AL (1997) Reliability and validity of MRI measurement of the amygdala and hippocampus in children with fragile X syndrome. *Psychiatr Res Neuroimag* 75:31–48

Killiany RJ, Moss MB, Nicholson T, Jolez F, Sandor T (1997) An interactive procedure for extracting features of the brain from magnetic resonance images: the lobes. *Hum Brain Map* 5:355–363

Kirk RE (1982) *Experimental design: procedures for the behavioral sciences*. Pacific Grove: Brooks/Cole

Koepp MJ, Richardson MP, Labbe C, Brooks DJ, Cunningham VJ, Ashburner J, VanPaesschen W, Revesz T, Duncan JS (1997) C-11-flumazenil PET, volumetric MRI, and quantitative pathology in mesial temporal lobe epilepsy. *Neurology* 49:764–773

Koeppe RA, Holthoff VA, Frey KA, Kilbourn MR, Kuhl DE (1991) Compartmental analysis of [^{11}C]flumazenil kinetics for the estimation of ligand transport rate and receptor distribution using positron emission tomography. *J Cereb Blood Flow Metab* 11:735–744

Laihinen AO, Rinne JO, Ruottinen HM, Nagren KA, Lehikoinen PK, Oikonen VJ, Ruotsalainen UH, Rinne UK (1994) PET studies on dopamine D1 receptors in the human brain with carbon-11-SCH 39166 and carbon-11-NNC 756. *J Nucl Med* 35:1916–1920

Lammertsma AA, Bench CJ, Hume SP, Osman S, Gunn K, Brooks DJ, Frackowiak RS (1996) Comparison of methods for analysis of clinical [^{11}C]raclopride studies. *J Cereb Blood Flow Metab* 16:42–52

Landlaw EM, DiStefano JJ III (1984) Multiexponential, multicompartmental, and noncompartmental modeling. II. Data analysis and statistical considerations. *Am J Physiol* 246:R665–R677

Laruelle M, Sidhu A, Casanova MF, Weinberger DR, Kleinman JE

(1991) Characterization of [^{125}I]SCH23982 binding in human brain: comparison with [^{3}H]SCH23390. *Neurosci Lett* 31:273–276

Laruelle M, Abi-Dargham A, Al-Tikriti MS, Baldwin RM, Zea-Ponce Y, Zoghbi SS, Charney DS, Hoffer PB, Innis RB (1994*a*) SPECT quantification of [^{123}I]iomazenil binding to benzodiazepine receptors in nonhuman primates. II. Equilibrium analysis of constant infusion experiments and correlation with *in vitro* parameters. *J Cereb Blood Flow Metab* 14:453–465

Laruelle M, Al-Tikriti MS, Zea-Ponce Y, Zoghbi SS, Baldwin RM, Charney DS, Hoffer PB, Kung HF, Innis RB (1994*b*) In vivo quantification of dopamine D2 receptors parameters in nonhuman primates with [^{123}I]iodobenzofuran and single photon emission computerized tomography. *Eur J Pharmacol* 263:39–51

Laruelle M, Baldwin RM, Rattner Z, Al-Tikriti MS, Zea-Ponce Y, Zoghbi SS, Charney DS, Price JC, Frost JJ, Hoffer PB, Innis RB (1994*c*) SPECT quantification of [^{123}I]iomazenil binding to benzodiazepine receptors in nonhuman primates. I. Kinetic modeling of single bolus experiments. *J Cereb Blood Flow Metab* 14:439–452

Laruelle M, van Dyck C, Abi-Dargham A, Zea-Ponce Y, Zoghbi SS, Charney DS, Baldwin RM, Hoffer PB, Kung HF, Innis RB (1994*d*) Compartmental modeling of iodine-123-iodobenzofuran binding to dopamine D_2 receptors in healthy subjects. *J Nucl Med* 35:743–754

Laruelle M, Wallace E, Seibyl JP, Baldwin RM, Zea-Ponce Y, Zoghbi SS, Neumeyer JL, Charney DS, Hoffer PB, Innis RB (1994*e*) *Graphical, kinetic and equilibrium analysis of [^{123}I]β-CIT in vivo* binding to dopamine transporters in healthy subjects. *J Cereb Blood Flow Metab* 14:982–994

Levenberg K (1944) A method for the solution of certain problems in least squares. *Q Appl Math* 2:164–168

Logan J, Fowler J, Volkow ND, Wolf AP, Dewey SL, Schlyer DJ, MacGregor RR, Hitzermann R, Bendriem B, Gatley SJ, Christman DR (1990) graphical analysis of reversible radioligand binding from time-activity measurements applied to [*N*-^{11}C-methyl]-(−)-cocaine PET studies in human subjects. *J Cereb Blood Flow Metab* 10:740–747

Logan J, Fowler JS, Volkow ND, Wang GJ, Ding YS, Alexoff DL (1996) Distribution volume ratios without blood sampling from graphical analysis of PET data. *J Cereb Blood Flow Metab* 16: 834–840

Meador-Woodruff JH, Damask SP, Wang J, Haroutunian V, Davis K, Watson SJ (1996) Dopamine receptors mRNA expression in human striatum and neocortex. *Neuropsychopharmacology* 15:17–29

Mintun MA, Raichle ME, Kilbourn MR, Wooten GF, Welch MJ (1984) A quantitative model for the in vivo assessment of drug binding sites with positron emission tomography. *Ann Neurol* 15:217–227

Munson P, Rodbard D (1980) LIGAND: a versatile computerized approach for characterization of ligand binding systems. *Ann Biochem* 107:220–239

Okubo Y, Suhara T, Suzuki K, Kobayashi K, Inoue O, Terasaki O, Someya Y, Sassa T, Sudo Y, Matsushima E, Iyo M, Tateno Y, Toru M (1997) Decreased prefrontal dopamine D1 receptors in schizophrenia revealed by PET. *Nature* 385:634–636

Otmakhova NA, Lisman JE (1996) D1/D5 dopamine receptor activation increases the magnitude of early long-term potentiation at CA1 hippocampal synapses. *J Neurosci* 16:7478–7486

Pani L, Gessa GL, Carboni S, Portas CM, Rossetti ZL (1990) Brain dialysis and dopamine: does the extracellular concentration of dopamine reflect synaptic release? *Eur J Pharmacol* 180:85–90

Rousset OG, Ma Y, Evans AC (1998) Correction for partial volume effects in PET: principle and validation. *J Nucl Med* 39:904–911

Sawaguchi T, Goldman-Rakic PS (1994) The role of D1-dopamine receptor in working memory: local injections of dopamine antagonists into the prefrontal cortex of rhesus monkeys performing an oculomotor delayed-response task. *J Neurophysiol* 71:515–528

Seamans JK, Floresco SB, Phillips AG (1998) D-1 receptor modulation of hippocampal-prefrontal cortical circuits integrating spatial memory with executive functions in the rat. *J Neurosci* 18:1613–1621

Seeman P (1992) Dopamine receptor sequences. Therapeutic levels of neuroleptics occupy D2 receptors, clozapine occupies D4. *Neuropsychopharmacology* 7:261–284

Seibyl JP, Laruelle M, van Dyck CH, Wallace E, Baldwin RB, Zoghbi SS, Zea-Ponce Y, Neumeyer JL, Charney DS, Hoffer PB, Innis RB (1995) Reproducibility of iodine-123-β-CIT SPECT brain measurement of dopamine transporters in healthy human subjects. *J Nucl Med* 37:222–228

Smith GS, Price JC, Lopresti BJ, Huang Y, Simpson N, Holt D, Mason NS, Meltzer CC, Sweet RA, Nichols T, Sashin D, Mathis CA (1998) Test-retest variability of serotonin 5-HT2A receptor binding measured with positron emission tomography and [^{18}F]altanserin in the human brain. *Synapse* 30:380–392

Talairach J, Tournoux P (1988) *Co-planar stereotactic atlas of the human brain. Three-dimensional proportional system: an approach of cerebral imaging.* New York: Theime Medical

Volkow ND, Fowler JS, Wang GJ, Dewey SL, Schyler D, MacGregor R, Logan J, Alexoff D, Shea C, Hitzemann R, Angrist B, Wolf AP (1993) Reproducibility of repeated measures of carbon-11-raclopride binding in the human brain. *J Nucl Med* 34:609–613

Wang GJ, Volkow ND, Levy AV, Fowler JS, Logan J, Alexoff D, Hitzemann RJ, Schyler DJ (1996) MR-PET image coregistration for quantitation of striatal dopamine D2 receptors. *J Comput Assist Tomogr* 20:423–428

Wienhard K, Eriksson L, Grootoonk S, Casey M, Pietrzyk U, Heiss WD (1992) Performance evaluation of the positron scanner ECAT EXACT. *J Comput Assist Tomgr* 16:804–813

Williams GV, Goldman-Rakic PS (1995) Modulation of memory fields by dopamine D1 receptors in prefrontal cortex. *Nature* 376:572–575

Woods RP, Cherry SR, Mazziotta JC (1992) Rapid automated algorithm for aligning and reslicing PET images. *J Comput Assist Tomogr* 16:620–633

Woods RP, Mazziotta JC, Cherry SR (1993) MRI-PET registration with automated algorithm. *J Comput Assist Tomogr* 17:536–546